THE ROTATIONAL RAMAN EFFECT: MOLECULAR

IMPURITIES IN ALKALI HALIDES

By

R. Callender and P. S. Pershan

Technical Report No. ARPA-39

Contract ARPA SD-88

January 1970

Submitted to:

Advanced Research Projects Agency

The Department of Defense

Division of Engineering and Applied Physics

Harvard University

Cambridge, Massachusetts

BLANK PAGE

THE ROTATIONAL RAMAN EFFECT: MOLECULAR IMPURITIES IN ALKALI HALIDES[*]

By

R. Callender[+] and P. S. Pershan

Division of Engineering and Applied Physics

Harvard University   Cambridge, Massachusetts

ABSTRACT

Raman scattering of light from representative alkali halide crystals containing CN^-, NO_2^-, OH^- and OD^- impurities is reported and analyzed. The observed spectra have a low frequency range, in which the scattered light is usually shifted from the incident light by less than 300 to 400 cm^{-1}, and a high frequency range in which the shifts are typically 1000 to 2000 cm^{-1}. Although the low frequency region does not readily lend itself to quantitative analysis it is clear that its main features can be interpreted in terms of a mixture of second order scattering from the pure host, impurity induced first order scattering that results from perturbing the pure host, and scattering from the rotational degrees of freedom of the molecular impurity.

The high frequency region, on the other hand, consists of spect whose frequencies are characteristic of the internal normal

coordinates of the molecule. A very narrow totally polarized line with depolarized sideband structure is generally observed. The sharp central component is at the frequency of an internal molecular normal coordinate and, typically, has a linewidth of one cm^{-1}. It is little affected by the type of host or changes in temperature. It is found that the sideband structure gives a measure of the molecular rotational dynamics. Depending on host and impurity, the observed characteristic behavior varies from nearly free rotation to heavily trapped librational motion.

The techniques employed here, both theoretical and experimental, demonstrate and define the rather broad usefulness of the Raman effect in studying systems of an analogous nature as in, for instance, molecular motion in liquids and liquid crystals as well as molecules in solids.

I. Introduction

In this paper we discuss the application of spontaneous Raman scattering techniques to the study of rotational motions of molecules. Although the systems studied were restricted to selected molecular impurities in various alkali halide single crystals, the results suggest that observations and analysis similar to what we report here will enable one to also study rotational motions of other molecular systems, including liquids.[1] The particular impurities and host crystals chosen for detailed examination were CN^- in KCl, KBr and NaCl as well as OH^- and OD^- in KCl. In addition less extensive observations were made on these same molecules in other hosts and also on NO_2^- in representative crystals. The choice of these systems for the present work was partially made on the basis that they had previously been studied by a variety of other methods and although a good deal was already known of their rotational kinetics, a number of questions had not yet been satisfactorily answered.[2-13] The consistency between conclusions drawn from the present measurements and previously published results of others is some measure of the general suitability of Raman scattering for quantitative measurements of molecular rotations.

Extensive studies; including near infrared absorption, stress, and specific heat measurements, have been performed by Seward and Narayanamurti on CN^- doped samples.[2] The detailed structure of the absorption bands in the vicinity of the internal stretching mode of the CN^- molecule (near 2000 cm^{-1}) was used to determine some features of the molecular rotational motion. The conclusion was that the CN^-

molecule in KC1, KBr, and RbCl is a relatively free rotator which could be successfully treated by the Devonshire model.[14] In the case of CN⁻ in NaC1 and NaBr, the results were inconclusive, but it was supposed the molecule is relatively heavily trapped in a given orientation. Vacancy and entropy studies showed that the CN⁻ molecule generally substitutes for the anion of the host. Stress measurements indicated that the minimum energy directions for the CN⁻ molecule are along ⟨100⟩ directions of the crystal.

Near infrared absorption stuides in the vicinity of the OH⁻ stretching mode (~ 3600 cm⁻¹) have been reported by Klein and co-workers.[3,4] Structure on this absorption band was interpreted to suggest that the molecule has lower energy excitations: one near 300 cm⁻¹ and one near 30 cm⁻¹. These two excitations together with the ground state splittings, have been found to be inconsistent with the simple Devonshire model.[3] The "30 cm⁻¹" excitation has been directly seen as an absorption band in the far infrared by Bosomworth for a few OH⁻ doped systems.[5] The 30 cm⁻¹ excitations can also be correlated with observed changes of the thermal conductivity of OH⁻ doped samples.[3] The ground state tunneling splittings of KCl:OH⁻ have been estimated using paraelectric resonance by Bron and Dreyfus,[6] Feher et al,[7] and Shearer and Estle.[8] Direct microwave absorption measurements of the tunneling levels in KCl:OH⁻ and NaCl:OH⁻ have been performed by Scott.[9] He has speculated that an extra term in the Devonshire expansion of the crystal potential can be used to explain the tunneling levels as well as the 30 cm⁻¹ and 300 cm⁻¹ excitations. Measurements of electric field induced dichroisms in the OH⁻ U.V. absorption bands have indicated the hydroxyl

ion substitutionally replaces an anion of the host with equilibrium directions of the molecule's axis pointing along $\langle 100 \rangle$ directions.[10-12]

Narayanamurti et al[13] have made extensive infrared and thermal conductivity measurements on alkali halide systems doped with NO_2^- and NO_3^-. In the $NaCl:NO_2^-$ system, the molecule is heavily trapped performing only a small librational motion even at room temperature. For $KCl:NO_2^-$ and $KBr:NO_2^-$, energy levels corresponding to free rotation, libration, and tunneling were found. In the $KI:NO_2^-$ system, considerable translational motion was suspected. In general for NO_2^- the C_2 axis of the molecule (this system has a bent structure like H_2O) was found to lie along $\langle 110 \rangle$ crystal axes directions in its equilibrium configuration.

The organization of the paper is as follows. The next section contains some theoretical considerations applicable to the particular systems studied here. In addition the formulism that was found to be most convenient for a detailed discussion of the experimentally observed light scattering properties of molecular impurities is specified. The formulism in this section will be kept as general as possible since we believe its convenient form is directly applicable to a large variety of other physical systems. Section III contains a description of the important components of the experimental apparatus as well as a description of the samples used in this study. The experimental results are discussed in sections IV and V. Here specific physical models for each impurity host system will be given. The formulism described in section II will be employed in order to relate the proposed models for the impurity motions to the observed spectral features. The discussion in section IV will concern only low frequency scattering (< 500 cm^{-1}) where the internal

normal coordinates of the molecule are not excited. This is found to be not very useful in understanding molecular rotational motion. In section V we will discuss higher frequency scattering (~ 1000 cm^{-1}) in the vicinity of the eigen frequencies of the internal normal coordinates. Sidebands accompanying the Raman scattering of the internal normal modes give quite detailed information on the molecular rotational motion.

II. Theoretical Consideration

A. Scattering Equations

The scattering theory used here is based on a semiclassical approach that has been described by a number of authors.[15-19] Although effect of the finite optical wavelength is neglected, this can be justified and the theory has yielded good results for Raman scattering of all orders for crystals of the rock salt structure as well as others. One may assume the Raman scattering is due to an ensemble average of identical molecules that do not interact with each other multiplied by the total number of molecules, n, which takes part in the scattering. Then, following Born,[16] the intensity of scattered radiation per solid angle, frequency shifted by ω from the laser centered at ω_0, is given by

$$I(\omega) = \frac{\eta(\omega_0 + \omega)^4}{2\pi c^3} \sum_{ijk\ell} n_i n_j I_{ik,j\ell}(\omega) E_k^- E_\ell^+ \qquad (2\text{-}1)$$

where c is the speed of light, n is the unit vector describing the polarization of the scattered radiation, and $(E^+)_\ell$ and $E^-)_k = (E^+)_k^*$ are the ℓ and k components of the amplitudes of the positive and negative frequency components of the incident radiation's electric field. The functions $I_{ik,k\ell}(\omega)$ are fourth rank tensor expressed by

$$I_{ik,j\ell}(\omega) = \sum_{nm} Z^{-1} \exp(-E_m/hT)\langle n|\alpha_{ik}|m\rangle\langle m|\alpha_{j\ell}|n\rangle \delta(\omega - k^{-1}(E_m - E_n)) \quad (2-2)$$

where m and n denote the eigenstates of the approximate Hamiltonian that is taken to represent vibrational and rotational motions of the molecule and its environment and Z is the partition function associated with these eigenstates. Viewing the polarizability $\underset{\sim}{\alpha}$ as a time dependent operator in the Heisenberg representation, this equation can also be written as[19]

$$I_{ik,j\ell}(\omega) = 2\pi^{-1} \int_{-\infty}^{\infty} dt \, e^{-i\omega t} \langle \alpha_{j\ell}(t)\alpha_{ik}(0)\rangle \quad (2-3)$$

where the brackets denote a thermal average. Under the assumption that the exciting frequency, ω_0, is not near any absorption band of the molecular scatterer, $\alpha_{j\ell}$ is taken to be a real, symmetric tensor. In this case the $I_{ik,j\ell}$ from Eq. (2-3) satisfy $I_{ik,j\ell} = I_{ki,j\ell} = I_{ik,\ell j}$ and $I_{ik,j\ell} = I_{j\ell,ik}$. Since it has been assumed that the measurements reflect a large number of scattering events from individual impurity centers (an ensemble average), the functions $I_{ik,j\ell}$ will transform according to the site symmetry of the environment of the impurity. For the particular systems here, the site symmetry is 0_h. Since the functions $I_{ij,k\ell}$ have the same symmetry properties as the elastic constants, one can make use of the well known properties of the elastic tensors for cubic crystals to demonstrate that for the 0_h point group there are only three independent functions namely $I_{xx,xx}(\omega)$, $I_{xx,yy}(\omega)$, and $I_{xy,xy}(\omega)$.[20] The x, y, z laboratory are chosen to coincide with the $\langle 100 \rangle$ axes of the host.

In general the time dependence of the $a_{ij}(t)$ is far to complicated to discuss without some simplifying assumptions. For the particular systems studied here, the observations are consistent with the assumption that the internal vibrational coordinates of the molecule do not couple to either the rotational or translational motion of the molecule as a whole, nor to the vibrational coordinates of the medium surrounding the molecule. Clearly, this assumption is not rigorously true; nevertheless, for the systems studied here, the observed Raman spectra do not appear to be significantly influenced by this coupling. Without claiming this assumption to be generally true for all systems, it is clear that the systems studied here are not unique in this respect. Where ever else this assumption proves to be applicable the techniques described here will yield direct information on the rotational motion of molecules. It remains for future research to determine just how widely it will be applicable. Under this assumption the polariz.bility associated with an isolated impurity molecule can be represented in the form

$$a_{ij} = a^0_{ij} + \sum_{v=1}^{r} [\partial a_{ij}/\partial Q^v]_{Q^v=0} Q^v . \tag{2-4}$$

The term a^0_{ij} describes contributions to the polarizability tensor arising from the orientation of the rigid molecule (i. e. neglecting the internal vibrational coordinates), the translation motion of the molecule's center of mass, and the interaction between these and the vibrational coordinates of the media surrounding the molecule. The $\{Q^v\}$ for $v = 1,....,r$ represent the internal vibrational coordinates of the molecule, assuming there are "r" of them. The coefficients $[\partial a_{ij}/\partial Q^v]_{Q^v=0}$ are assumed to be solely dependent

on the molecule; and, in the molecule's reference frame "MF", these are just constants.

We may write the general eigenstates that appear in Eq. (2-2) in the form $|n\rangle = |\xi\rangle \prod_{\nu=1}^{r} |N_\nu\rangle$ where the $\{|N_\nu\rangle\}$ are simple harmonic oscillator wave functions appropriate to the internal molecular mode Q^ν and $|\xi\rangle$ designates all other quantum numbers of the system including the orientational and the other vibrational coordinates of the impurity-host system. In order to consider scattering where only one of the N_ν changes by $+1$, i.e. Stokes scattering in the vicinity of an internal molecular mode, defin:

$$\alpha^\nu_{ij} \equiv [\partial\alpha_{ij}/\partial Q^\nu]_{Q^\nu=0} Q^\nu . \tag{2-5}$$

Then the matrix element $\alpha^\nu_{ij}(MF) \equiv \langle N_\nu = 0|\alpha^\nu_{ij}|N_\nu = 1\rangle$ (2-6)

is a constant when the coordinates (ij) refer to the molecular frame of reference, MF. It is not necessary to calculate the numerical values for the $\{\alpha^\nu_{ij}(MF)\}$; their from follows directly from symmetry considerations. [15, 17]

In order to calculate the Raman spectrum from Eq. (2-2), these tensors must be rotated into the laboratory frame which, in all cases, will be defined by the $\langle 100\rangle$ axes of the host. In a more complete calculation, it would also be necessary to take into account the translational motion of the molecule. For our purposes, it can be shown that to a good approximation the translational motion can be neglected in the present discussion. [21] The effect of this is that in discussing models of the possible types of molecular motion, all models which have equivalent rotational motion, regardless of the translational motions, predict the

same spectra for Raman scattering in the vicinity of an internal stretching mode.

In cases where $\alpha^\vee_{ij}(MF)$ is not isotropic the polarizability of the molecule as seen in the laboratory frame is a function of the Eulerian angles that relate the MF frame to the laboratory frame. Schematically denoting these angles by Ω the rotation of $\alpha^\vee_{ij}(MF)$ into the laboratory frame can be written formally as

$$\underset{\sim}{\alpha}^\vee = \underset{\sim}{R}(\Omega)\underset{\sim}{\alpha}^\vee(MF)\underset{\sim}{R}^+(\Omega) . \tag{2-7}$$

where $\underset{\sim}{R}(\Omega)$ is the appropriate rotation matrix. We then have that the Stokes scattering in the vicinity of the νth stretching mode has the following form in the Schrodinger picture.

$$I^\vee_{ik,j\ell}(\omega) = \sum_{\xi\xi'} (Z'Z_{int})^{-1} \exp(-E_\xi/kT)\langle\xi'|\alpha^\vee_{ik}|\xi\rangle\langle\xi|\alpha^\vee_{j\ell}|\xi'\rangle$$
$$\times \delta[(\omega + \omega_\nu - \hbar^{-1}(E_\xi - E_{\xi'})] \tag{2-8}$$

where the labels ξ' and ξ define the rotational and vibrational eigenstates which do not include the molecular internal modes.

The $\alpha^\vee_{ij}$ in Eq. (2-8) are related to the $\alpha^\vee_{ij}(MF)$ defined by Eq. (2-6) through the unitary transformation specified by Eq. (2-7). The eigenfrequency of the νth mode is ω_ν. In the Heisenberg picture

$$I^\vee_{ik,j\ell}(\omega) = \frac{1}{2\pi} \int_{-\infty}^{\infty} dt \exp[-it(\omega + \omega_\nu)]\langle\alpha^\vee_{j\ell}(t)\alpha^\vee_{ik}(0)\rangle \tag{2-9}$$

where the time dependence of $\alpha^\vee_{j\ell}(t)$ is just the time dependence that results from transforming Eq. (2-6) into the laboratory frame of reference.

It is a matter of the convenience of a particular calculation as to the choice of either Eq. (2-8) or (2-9). In general if explicit knowledge of the

wave functions of the system are known, then the Schrodinger form of the polarizability used in conjunction with Eq. (2-8) will exactly define the scattering results. However, in many cases this type of information is not available and then the Heisenberg formulation of (2-9) may be more useful. In particular it is often possible to exploit the formal similarity of this scattering equation with its classical analog in which case the brackets are interpreted as a corrrelation function and treat the motion of the molecule by classical or semiclassical arguments. This serves in many cases to give a reasonable description of the experimental results. It may be noted the rotation matrices $\underset{\sim}{R}(\Omega)$ of Eq. (2-7) are time independent when viewed in the Schrodinger picture or time dependent in the Heisenberg picture. In this latter case, we have explicitly

$$\underset{\sim}{\alpha}^{\nu}(t) = \underset{\sim}{R}(\Omega(t))\underset{\sim}{\alpha}^{\nu}(MF)\underset{\sim}{R}^{+}(\Omega(t)) . \qquad (2-10)$$

These rotation matrices are rather involved, and for this work it has been found to be more convenient to treat each impurity host system separately as a special case where some symmetry argument could be exploited. A representation of the general form of Eq. (2-7) in terms of the Eulerian angles is given later in this section.

A simplification of Eq. (2-9) can be made as follows:

$$\underset{\sim}{\alpha}^{\nu}(MF) = \overline{\alpha}^{\nu}\underset{\sim}{I} + \underset{\sim}{\beta}^{\nu}(MF) \qquad (2-11a)$$

where

$$\overline{\alpha}^{\nu} = \frac{1}{3}\mathrm{Tr}\,\underset{\sim}{\alpha}^{\nu}(MF)$$

$$\mathrm{Tr}\,\underset{\sim}{\beta}^{\nu}(MF) = 0 \qquad (2-11b)$$

and $\underset{\sim}{I}$ is the identity matrix. Any second rank tensor may be so decomposed. Using Eq. (2-10), we have

$$\underset{\sim}{\alpha}^{v}(t) = \bar{\alpha}^{v}\underset{\sim}{I} + \underset{\sim}{\epsilon}^{v}(t) \tag{2-12a}$$

$$\underset{\sim}{\epsilon}^{v}(t) = \underset{\sim}{R}(\Omega(t))\underset{\sim}{\epsilon}^{v}(M^{-1}\underset{\sim}{R}^{+}(\Omega(t))) . \tag{12-12b}$$

The scattering is described in terms of the Fourier transform of the correlation functions

$$\langle \underset{\sim}{\alpha}^{v}(t)\underset{\sim}{\alpha}^{v}(0)\rangle = (\bar{\alpha}^{v})^{2} + \bar{\alpha}^{v}\underset{\sim}{I}\langle\underset{\sim}{\epsilon}^{v}(0)\rangle$$
$$+ \langle\underset{\sim}{\epsilon}^{v}(t)\rangle\underset{\sim}{I}\bar{\alpha}^{v} + \langle\underset{\sim}{\epsilon}^{v}(t)\underset{\sim}{\epsilon}^{v}(0)\rangle . \tag{2-13}$$

Now $\langle\underset{\sim}{\epsilon}^{v}(t)\rangle$ is a second rank tensor which must be invariant under all operations of O_h symmetry. In this case it is easy to show that any second rank tensor must be proportional to the identity matrix. This taken with the fact that $\text{Tr }\underset{\sim}{\epsilon}^{v}(t) = 0$ (this holds for all times as can be seen by noting Eq. (2-11b) and also that the trace is invariant under unitary transformation) implies that $\langle\underset{\sim}{\epsilon}(t)\rangle = \langle\underset{\sim}{\epsilon}(0)\rangle = 0$. Thus

$$\langle\alpha^{v}_{j\ell}(t)\alpha^{v}_{ik}(0)\rangle = (\bar{\alpha}^{v})^{2}\delta_{j\ell}\delta_{ik} + \langle\epsilon^{v}_{j\ell}(t)\epsilon^{v}_{ik}(0)\rangle \tag{2-14}$$

and we have from Eq. (2-9)

$$I^{v}_{ik,j\ell}(\omega) = (\bar{\alpha}^{v})^{2}\delta_{ik}\delta_{j\ell}\delta(\omega + \omega')$$
$$+ 2\pi^{-1}\int_{-\infty}^{\infty} dt\, \exp[-it(\omega + \omega_{v})]\langle\epsilon^{v}_{j\ell}(t)\epsilon^{v}_{ik}(0)\rangle \tag{2-15}$$

where δ_{ij} is the Kroniker delta function. There are, then, in cases where the polarizability of a particular internal mode is nonzero, two components to the scattering for O_h point site symmetry. The first is centered at the frequency of the stretching mode and is not broadened by the rotational motion. This has been called by a variety of terms

including trace scattering and the "Q(0)" branch. Taking note of the Kroniker delta functions, the trace scattering is totally polarized, parallel to the electric field of the incident light, and is independent of crystal orientation.

The second half of Eq. (2-15) arises from the traceless components of the polarizability tensor and is modulated by the motion of the molecule. Since the brackets represent an ensemble average, it is evident again following the arguments discussed above that $\langle \beta^{\nu}_{j\ell}(t)\beta^{\nu}_{ik}(0)\rangle$ is invariant under O_h symmetry; and, thus, the only independent quantities are $\langle \beta^{\nu}_{xx}(t)\beta^{\nu}_{xx}(0)\rangle$, $\langle \beta^{\nu}_{xx}(t)\beta^{\nu}_{yy}(0)\rangle$ and $\langle \beta^{\nu}_{xy}(t)\beta^{\nu}_{xy}(0)\rangle$ (again ensemble averages with the obvious permutation of the indices are identical). In this case, however, since $\mathrm{Tr}\,\underset{\approx}{\beta}(t) = 0$

$$
\begin{aligned}
0 &= \langle(\beta^{\nu}_{xx}(t) + \beta^{\nu}_{yy}(t) + \beta^{\nu}_{zz}(t))\beta^{\nu}_{yy}(0)\rangle \\
&= 2\langle \beta^{\nu}_{xx}(t)\beta^{\nu}_{yy}(0)\rangle + \langle \beta^{\nu}_{xx}(t)\beta^{\nu}_{xx}(0)\rangle.
\end{aligned}
\tag{2-16}
$$

Therefore, following from Eq. (2-16) the second component of Eq. (2-15) predicts only two independent spectral functions in addition to the trace scattering δ-function. We shall consistently express the results here in terms of $\langle \beta^{\nu}_{xx}(t)\beta^{\nu}_{xx}(0)$ and $\langle \beta^{\nu}_{xy}(t)\hat{\beta}^{\nu}_{xy}(0)\rangle$.

The scattering in the vicinity of a stretching mode then conveniently divides into three terms. Experimentally the narrow trace scattering can be used to locate the position of the stretching mode. It is also very useful in probing the extent to which the theory holds. The predicted linewidth is zero and departures from this are a direct measure of the approximations used here. The other two scattering functions are a measure of the rotational motion of the molecule. As defined by

specific models, tumbling times if appropriate can be measured from the bandwidth of the Raman results.

The three terms can be isolated by choosing appropriate scattering geometries. The details for this are tabulated in Table 2-1 where several of the most convenient geometries are given in terms of the crystal axes. It may be noted that the trace scattering cannot be completely isolated. However, in practice, since it is quite narrow, it is easily identified in an examination of the results. The other two scattering terms can be clearly isolated simply by using cases (2) and (4) of Table 2-1. As a practical matter due to finite solid angles and other effects, the Raman geometries are not precisely defined in performing the actual experiment, however, cases (2) and (4) were found to maximize the isolation of the two rotationally modulated terms and were most often used.

The discussion in this section has been almost exclusively in terms of the Raman scattering that originates in the internal stretching vibrations of the molecule itself. Since the internal energies of the molecules studied here are large (2000 cm^{-1} for CN$^-$, 3600 for OH$^-$, and 800 cm^{-1} for the lowest frequency mode of NO$_2^-$) compared to rotational states of the free molecule or vibrational states of the impure host, the scattering results from these two components can be experimentally separated. Thus, there are two different, clearly definable spectral regions: low frequency scattering and high frequency scattering in the vicinity of the stretching modes; the spectra from the two sources are fundamentally different.

As defined by Eqs. (2-8) and (2-9), the sideband data are a measure of the tumbling or rotational-like motion of the molecule itself.

Case	$\hat{E}_0$	$\hat{k}_0$	$\hat{E}_s$	$\hat{k}_s$	Intensity Proportional to
1	$\frac{1}{\sqrt{2}}(110)$	$\frac{1}{\sqrt{2}}(1\bar{1}0)$	$\frac{1}{\sqrt{2}}(110)$	(001)	$(\bar{\alpha}^\nu)^2 + \langle \beta^\nu_{xy}(t)\beta^\nu_{xy}(0)\rangle$ $+ \frac{1}{4}\langle \beta^\nu_{xx}(t)\beta^\nu_{xx}(0)\rangle$
2	$\frac{1}{\sqrt{2}}(110)$	$\frac{1}{\sqrt{2}}(1\bar{1}0)$	$\frac{1}{\sqrt{2}}(1\bar{1}0)$	(001)	$\frac{3}{4}\langle \beta^\nu_{xx}(t)\beta^\nu_{xx}(0)\rangle$
3	(100)	(010)	(100)	(001)	$(\bar{\alpha}^\nu)^2 + \langle \beta^\nu_{xx}(t)\beta^\nu_{xx}(0)\rangle$
4	(100)	(010)	(010)	(001)	$\langle \beta^\nu_{xy}(t)\beta^\nu_{xy}(0)\rangle$

$$\bar{\alpha}^\nu = \frac{1}{3}\,\mathrm{Tr}\,\underset{\approx}{\alpha}^\nu(MF)$$

Table 2-1: Scattering results for various geometries in the vicinity of a stretching mode. $\hat{E}_0$ and $\hat{k}_0$ are unit vectors describing the directions of the polarization and propagation of the incident light field, respectively, with $\hat{E}_s$ and $\hat{k}_s$ analogously defined for the scattered light. See text for a discussion of the various terms in the scattering. The directions of $\hat{k}_0$ and $\hat{k}_s$ have been listed for convenience and do not influence the scattering results.

The details of the interaction between the host and the molecule will determine the tumbling motion [examine, for example, Eq. (2-10)]. However, no matter how complicated the motion, is, the Raman cross section in the vicinity of the stretching mode is a projection of the tumbling motion of the molecule only. The low frequency scattering, on the other hand, is much harder to interpret. For example, the calculation of the Raman cross section which involves a rotational motion of the molecule with a simultaneous motion of host ions must include the whole complex. To further complicate matters, the low frequency results will also include the rather large normal second order Raman scattering of the pure alkali halide (these crystals have no first order allowed scattering) as well as scattering from phonon-like modes which do not include the rotational motion of the molecule.

In the special case where quantum states may be separately labeled as to modified rotational states and modified host phonon states, the low frequency scattering results can be labeled by normal second order, induced first order, and molecular rotational scattering. The induced first order scattering is a result of the k selection rule becoming somewhat relaxed by the presence of the impurity. For spherical impurities in alkali halides, this effect has been calculated by Xinh,[18] Maradudin,[19] and others.[22, 23] Their results will be used in section IV when the low frequency results are given.

One further theoretical point to be noted for this special case, where there are separate rotational and modified phonon states, is that there is a relationship between the sideband spectra and the low frequency scattering spectra due to rotational-like motion of the rigid molecule.

If the symmetry of the internal mode is the same as that of the molecule, then the shape and form of the two scattering spectra are identical since in the molecular frame the forms of the polarizability tensors for the rigid molecule and for the α^v_{ij} are identical apart from a constant factor. To be specific, viewing the polarizability as a Heisenberg operator, we are interested in quantities like $\langle \underset{\sim}{\alpha}^v(t)\underset{\sim}{\alpha}^v(0)\rangle$ in the vicinity of the stretching mode and $\langle \underset{\sim}{\alpha}^0(t)\underset{\sim}{\alpha}^0(0)\rangle$ for the low frequency results where $\underset{\sim}{\alpha}^0(t)$ denotes the polarizability of the molecule at time t in its ground vibration state. We have $\underset{\sim}{\alpha}^v(t) = \underset{\sim}{R}(\Omega(t))\underset{\sim}{\alpha}^v(MF)\underset{\sim}{R}^+(\Omega(t))$ and a similar expression for $\alpha^0(t)$. Since the stretching mode is assumed not to perturb the rotational motion, the rotation matrices involved for both $\underset{\sim}{\alpha}^v(t)$ and $\underset{\sim}{\alpha}^0(t)$ are equal. Then if $\underset{\sim}{\alpha}^v(MF) = D\underset{\sim}{\alpha}^0(MF)$ where D is a constant, the functional form of the two correlation functions are equal. Examining Eqs. (2-8) and (2-9) it is evident the scattering spectra are the same apart from a shift in origin due to the stretching mode frequency and the constant factor multiplying the intensity. For the molecules studied here, all the internal stretching modes except the B_1 mode of NO_2^- do preserve the symmetry of the molecule. Thus, except for this last case, a detailed comparison can be made between structure of the sideband data and structure of the low frequency data.

This theory can be extended to any molecular system where the internal normal coordinates are not coupled to other degrees of freedom. One would find a low frequency region where the Raman scattering would be due to a complicated sum of correlations functions between individual components of the system. The high frequency scattering, however, in the vicinity of a stretching mode would reflect the tumbling motion of a

single molecule. Nowhere in the development of the high frequency scattering have the details of our particular systems been exploited except in the development of the depolarized scattering symmetries due to the point symmetry of the molecule's site. These symmetry considerations are readily extendable to other point symmetries. In an isotropic liquid, for example. one would find only two scattering symmetries rather than three found for O_h symmetry. That is one in which the scattered light is polarized parallel to the incident electric field of the laser, which would include the trace scattering. and one depolarized spectra (polarized perpendicular to the electric field of the laser) which would be a measure of the molecular motion. For detailed expressions for this case, see ref. (24 and 25).

For reference, we conclude this section by listing the forms of the polarizability tensors in the molecular frames for the molecules studied here. We have for OH⁻ and CN⁻, one stretching mode

$$\alpha^{\nu}(MF) = \begin{pmatrix} a & & \\ & a & \\ & & b \end{pmatrix} \tag{2-17}$$

where the z axis is taken along the internuclear axis of the molecule. In the case of the NO_2^- impurity, there are three internal modes (see reference (13)) all of which are Raman active. The point group symmetry of the molecule is C_{2v}; two of the modes have A_1 symmetry and the third has B_1 symmetry. From Loudon,[17]

$$\alpha^{A_1}(MF) = \begin{pmatrix} a & & \\ & b & \\ & & c \end{pmatrix} \tag{2-18a}$$

$$\alpha^{B_1}(MF) = \begin{pmatrix} 0 & 0 & f \\ 0 & 0 & 0 \\ f & 0 & 0 \end{pmatrix} \tag{2-18b}$$

B. Angular Dependence of the Polarizability Tensor

The functional form of the molecular polarizability tensor in terms of the Eulerian angles can be derived in the following way. We have from Eq. (2-7)

$$\underline{\alpha}^V(\Omega) = \underline{R}(\Omega)\underline{\alpha}^V(MF)\underline{R}^+(\Omega) \tag{2-19}$$

Let $(\alpha\beta\gamma) \equiv (\Omega)$ be the Eulerian angles as defined by Edmonds.[26] Throughout this section, we shall use the definitions and normalizing conventions as given in ref. (26). For $\Omega = 0$ the moleuclar coordinate system coincides with the laboratory axes $\underline{\alpha}^V(0) = \underline{\alpha}^V(MF)$.

To perform the operations defined by (2-19), it is convenient to decompose $\underline{\alpha}^V(MF)$ into forms which have the transformation properties of irreducible tensor operators, $T(kq)$. These functions, for each k, form a set of $2k + 1$ operators ($q = -k, -k+1, \ldots, k-1, k$) which, under an arbitrary rotation, transform like

$$R(\Omega)T(kq)R^+(\Omega) = \sum_{q'=-k}^{k} T(kq')D^k_{q'q}(\Omega) . \tag{2-20}$$

The forms and symmetry properties of the $D^k_{q'q}(\Omega)$ are well known and form a convenient set of functions. Reference should be made to Edmonds[26] and Rose[27] for explicit properties of the $D^k_{q'q}(\Omega)$.

The components of a symmetric second rank tensor transform under rotations like bilinear combinations of x, y and z, i.e. α_{xy} transforms like xy. As defined in Edmonds, the solid harmonics, $Y_{\ell m}(\underline{r})$, are given by

$$Y_{\ell m}(\underset{\sim}{r}) = r^{\ell} Y^{m}_{\ell}(\theta, \varphi) \tag{2-21}$$

where $Y^{m}_{\ell}(\theta, \phi)$ are spherical harmonics, transform like $T(\ell m)$. The solid harmonics in terms of x, y, z functional forms can be found in Table 1 of Edmonds. For example, we have

$$Y_{20} = 4^{-1}(5/\pi)^{\frac{1}{2}}(2z^2 - x^2 - y^2) \tag{2-22}$$

Thus,

$$T(20) = 4^{-1}(5/\pi)^{\frac{1}{2}}(2\alpha_{zz} - \alpha_{xx} - \alpha_{yy}) \tag{2-23}$$

when the "equals sign" is taken to mean both sides of the equation have the same transformation properties. Examining Table 1 of Edmonds further, it is found

$$T(00) = 2^{-1}\pi^{-\frac{1}{2}}(\alpha_{xx} + \alpha_{yy} + \alpha_{zz}) \tag{2-24}$$

$$T(2\pm1) = \mp 2^{-1}(15/2\pi)^{\frac{1}{2}}(\alpha_{zx} \pm i\alpha_{zy})$$

$$T(2\pm2) = 4^{-1}(15/2\pi)^{\frac{1}{2}}(\alpha_{xx} - \alpha_{yy} \pm 2i\alpha_{xy}) .$$

The six independent components of a second rank tensor, $\underset{\sim}{\alpha}$, can be written as sums of $T(\ell q)$ by inverting the above equations. Defining the following matrices

$$\hat{\alpha}^{0}_{0} = (2/3)(\pi)^{\frac{1}{2}}\begin{pmatrix} 1 & & \\ & 1 & \\ & & 1 \end{pmatrix} \tag{2-25}$$

$$\hat{\alpha}^{2}_{0} = (2/3)(\pi/5)^{\frac{1}{2}}\begin{pmatrix} -1 & & \\ & -1 & \\ & & 2 \end{pmatrix}$$

$$\hat{\alpha}^{2}_{\pm1} = (2\pi/15)^{\frac{1}{2}}\begin{pmatrix} 0 & 0 & \mp1 \\ 0 & 0 & i \\ \mp1 & i & 0 \end{pmatrix}$$

$$\hat{\alpha}^{2}_{\pm2} = (2\pi/15)^{\frac{1}{2}}\begin{pmatrix} 1 & \mp i & 0 \\ \mp i & -1 & 0 \\ 0 & 0 & 0 \end{pmatrix}$$

we have

$$\underset{\sim}{\alpha} = T(0,0)\hat{\alpha}^0_0 + \sum_{m=-2}^{+2} T(2,m)\hat{\alpha}^2_m . \qquad (2-26)$$

The matrices $\hat{\alpha}^j_m$ can be viewed as projection matrices as they project out just the proper combinations of $\underset{\sim}{\alpha}$ that transform under rotations in the same way as irreducible tensor operators. Therefore, a rotation of $\underset{\sim}{\alpha}$ will change the $T(\ell m)$ in Eq. (2-26) as in (2-20).

Now, letting $\underset{\sim}{\alpha} = \underset{\sim}{\alpha}^\nu(0) = \underset{\sim}{\alpha}^\nu(MF)$, we have

$$\underset{\sim}{\alpha}^\nu(\Omega) = R(\alpha^\nu(0))R^+ = T^0(0,0)\hat{\alpha}^0_0 + \sum_{mm'} \hat{\alpha}^2_m T^0(2,m')D^2_{m'm}(\Omega) \qquad (2-27)$$

where $T^0(\ell m)$ are values multiplying the $\underset{\sim}{\alpha}^2_m$ when $\Omega = 0$. Note this formula reduces correctly at $\Omega = 0$. We have from Edr ; that $D^2_{m'm}(0) = \delta_{m'm}$.

For the case where $\underset{\sim}{\alpha}^\nu(MF)$ is diagonal with elements $\alpha^\nu_{xx}, \alpha^\nu_{yy}$, and $\underset{\sim}{\alpha}^\nu_{zz}$, (2-27) reduces to

$$\underset{\sim}{\alpha}^\nu(\Omega) = 3^{-1}(\alpha^\nu_{xx} + \alpha^\nu_{yy} + \alpha^\nu_{zz})\underset{\sim}{I}$$

$$+ 4^{-1}(5/\pi)^{\frac{1}{2}} \sum_m \hat{\alpha}^2_m [(2\alpha^\nu_{zz} - \alpha^\nu_{xx} - \alpha^\nu_{yy})D^2_{0m}(\Omega)$$

$$+ 3^{\frac{1}{2}}(\alpha^\nu_{xx} - \alpha^\nu_{yy})(D^2_{2m}(\Omega) + D^2_{-2m}(\Omega))] . \qquad (2-28)$$

C. Selection Rules

In general the wave functions for the rotating molecule can be labeled according to the irreducible representations of the molecule's point site symmetry. For a particular experimental scattering geometry, it can be expected that only certain of the Raman allowed transitions will

be seen. It is the purpose of this section to derive some rules governing this by examining the transformation properties of $\underset{\sim}{a}^V(\Omega)$.

Let Γ be the group of symmetry operators of the molecular site and Γ_R be the subgroup of Γ containing all the proper rotations of Γ. Associated with Γ_R are forms for a symmetric second rank tensor which will transform amongst themselves according to the irreducible representations of Γ_R. Let $\hat{u}^j_\mu$ be the jth representation and the μth component of the representation. The specific forms of $\hat{u}^j_\mu$ can be found in Loudon.[17] For the $O_h(m3m)$ group, for example, $\Gamma_R = O$ in the Schoenflies notation or 432 in the international short notation and the $\hat{u}^j_\mu$ consist of one A_1, two E, and three F_2 components. Expand $\underset{\sim}{a}^V(\Omega)$ as a sum of these tensors (six are needed, in general, as there are six independent elements of $\underset{\sim}{a}^V(\Omega)$). For an aribitrary Γ, some representations may be repeated. We have

$$a^V(\Omega) = \sum_{j,\mu} \hat{u}^j_\mu f^j_\mu(\Omega) \qquad (2\text{-}29)$$

where the angular factors are grouped into the functions $f^j_\mu(\Omega)$.

The $\hat{u}^j_\mu$ are defined by the laboratory (crystal) axes, and the experimental scattering geometry chooses which of the $\hat{u}^j_\mu$ will be observed. The selection rules are determined by the transformation properties of the $f^j_\mu(\Omega)$ since scattering between the rotational states S and S' will be allowed if $\langle S | f^j_\mu(\Omega) | S' \rangle$ is nonzero. We thus need to determine the properties of $f^j_\mu(\Omega)$.

Under the group Γ_R, except for groups with complex characters, the functions $f^j_\mu(\Omega)$ transform is the same way as $\hat{u}^j_\mu$. Consider the

following. Apply one of the symmetry rotations, P_R, to the crystal axes of the site. We have for $\underset{\sim}{\alpha}^\nu(\Omega)$

$$P_R \underset{\sim}{\alpha}^\nu(\Omega) = \sum_{\mu,\mu'} \hat{u}^j_{\mu'} P^j_{\mu'\mu}(R) f^j_\mu(\Omega) \qquad (2\text{-}30)$$

where $P^j_{\mu,\mu}(R)$ are the numbers describing the transformation properties of $\hat{u}^j_\mu$. If we now apply P_{-R} to the molecule, we must have the same physical situation. Thus, $P^{site}_R \underset{\sim}{\alpha}(\Omega) \equiv P^{molecule}_{-R} \underset{\sim}{\alpha}(\Omega)$, so that

$$P_{-R} f^j_\mu(\Omega) = \sum_{\mu'} f^j_{\mu'}(\Omega) P^j_{\mu'\mu}(+R) \qquad (2\text{-}31a)$$

or

$$P_R f^j_\mu(\Omega) = \sum_{\mu'} f^j_{\mu'}(\Omega) P^j_{\mu'\mu}(-R). \qquad (2\text{-}31b)$$

It is easy to show (ref. (28), p. 74) that

$$\left[P^j_{\mu\mu'}(R) \right]^* = P^j_{\mu'\mu}(-R) . \qquad (2\text{-}32)$$

Thus, if $\chi(R)$ is the character of $P_R(R)$, then

$$\chi^j(R) = \sum_\mu P^j_{\mu\mu}(R) = \sum_\mu \left[P^j_{\mu\mu}(-R) \right]^* , \qquad (2\text{-}33)$$

Omitting the few groups with complex characters, we have the result that $f^j_\mu(\Omega)$ transforms in the same way as $\hat{u}^j_\mu(\Omega)$ under the group Γ_R. [In the case of groups with complex characters $[f^j_\mu(\Omega)]^*$ transforms as $\hat{u}^j_\mu(\Omega)$ and the selection rules are slightly more complex]. If the experimental geometry specifies the $\hat{u}^j_\mu$ symmetry the only allowed Raman transitions are those in which the direct product of $|S\rangle$ with $|S'\rangle$ contains the $\hat{u}^j_\mu$ symmetry [for point groups with real $\chi^j(R)$].

To take into account further symmetry operators of the group $\tilde{}$, a crystal mirror plane, for example, it is necessary to have knowledge of the symmetry properties of the internal normal mode of the molecule. The reason for this is that these operations acting on the molecular frame may not result in the same physical situation as a mirror operation acting on the laboratory frame.

For the case of a linear molecule in 0_h symmetry where the $\underline{\alpha}^{\vee}(\Omega)$ refers to the single stretching mode, however, the functions $f^j_{\mu}(\Omega)$ do transform under the full operations of the 0_h point group as the $\hat{u}^j_{\mu}$. It has already been shown that $f^j_{\mu}(\Omega)$ transforms like A_1, E_1, and F_2 representations where the subscript μ is single valued, double valued, and triple valued respectively and, further, that $f^E_{\mu}(\Omega)$ multiplies $\hat{u}^E_{\mu}$ and similarly for the other two representations. Under 0_h, the matrices, $\hat{u}^j_{\mu}$, transform like A_{1g}, E_g, and F_{2g}. Performing the inversion operatior on the molecule, at any arbitrary Ω, gives the same polarizability tensor. Therefore, the functions $f^j_{\mu}(\Omega)$ are unchanged. Thus, $f^j_{\mu}(\Omega)$ transforms like A_{1g}, E_g, and F_{2g} as well. We thus have for this case that experiments which measure in turn $\hat{u}^j_{\mu}$, $j = A_{1g}$; $\hat{u}^j_{\mu}$, $j = E_g$ and $\hat{u}^j_{\mu}$, $j = F_{2g}$ only project out transitions whose cross product contains A_{1g}, E_g, and F_{2g} components respectively.

III. Equipment and Crystals

The Raman measurements were made employing right angle scattering techniques with an argon ion laser as the exciting source having one watt at 4880 $\overset{o}{A}$ and a Spex model 1400 double monochromator. The signal was electronically detected by a cooled EMI 9558

photo-multiplier and recorded by a photon counting scheme which has been previously described.[29] A Janis Super Vari-Temp Model 10-DT dewar was used for sample temperature control. This dewar is top loading, allowing sample changes with one helium fill, and works by blowing cold helium gas on the sample. The sample temperature can be changed either by heating the helium gas before it reaches the sample chamber to the appropriate value (which we found to be convenient for temperatures less than $30^{\circ}K$) or by heating the sample holder and balancing this against the cold helium gas (best method for temperature from ~ $30^{\circ}K$ to $300^{\circ}K$). The temperature of the sample block was monitored using one of two sensors. Most temperature measurements were made by a Phylatron Inc. (Columbus, Ohio) Gallium Arsenide diode model number CD-500A. A constant current supply (supplying only $20\mu A$ to avoid heating) in series with the diode created a voltage across the diode which varies with temperature. This voltage can be read with a potentiometer and typically a variation of 1-2 mv/$^{\circ}K$ is seen. The dynamic range of the diode is $1^{\circ}K$ to $300^{\circ}K$. Due to variations in recycling of the diode and calibration inaccuracies, the temperature could not be determined to within $\pm 2^{\circ}K$. This error, however, for nearly all the work reported here is insignificant. The second temperature sensor was used for the low temperature region (under $30^{\circ}K$), in cases where it was felt better accuracy was required. This sensor, a calibrated germanium resistor, was made by Cryocal (Riviera Beach, Florida, model number CR1000). Here an accuracy of $\pm .1^{\circ}K$ was easily obtainable. Unless otherwise stated, an absolute temperature inaccuracy of $\pm 2^{\circ}K$ should be assumed.

The width (full width at half intensity) of the "trace" lines of the CN$^-$ doped systems were measured using standard geometry $180°$ pressure scanning Fabry-Perot interferometer. The instrument linewidth of the Fabry-Perot was estimated using theoretical formulas for reflectivity, mirror flatness, and finite pinhole finesse. In addition it was found that the 4880 $\overset{o}{A}$ laser linewidth $(.14 \text{ cm}^{-1})$ was a significant fraction of the trace linewidth. The instrument linewidth was taken as the simple sum of these four linewidths. The trace linewidth was determined using a deconvolution process developed by W. Lacina[30] which assumes a triangular instrumental slit function. The measurements of the CN$^-$ doped systems are accurate to within 20%.

The NO$_2^-$ and CN$^-$ doped systems were made on samples grown by Gerhard Schmidt in the Laboratory of Atomic and Solid State Physics at Cornell University. In the case of the CN$^-$ systems, the main impurity is thought to be NCO$^-$. See reference (2) for details. Using the calibration numbers quoted in reference (2) for the absorption coefficients, the concentrations of NCO$^-$ were about two orders of magnitude less than the concentration of CN$^-$ in all cases. OH$^-$ and OD$^-$ doped samples were grown by Franz Rosenberger at the Crystal Growth Laboratory, University of Utah. The main impurity in these samples is thought to be several parts per million of $0^-{}_2$.[31]

The determination of the concentration of the dopant in any particular host was made by measuring the optical density of one of the internal modes and comparing these values against previously reported formulas giving concentration in terms of optical density. Reference may be made to Seward[2] for CN$^-$ systems, Narayanamurti[13] for NO$_2^-$.

Fritz et al.[32] for OH$^-$, and Wedding[4] for OD$^-$. This method of determining concentration is probably accurate to within 20%.

IV. Low Frequency Results

A. Data

The various spectral features described in this section have been labeled according to the symmetry of the transition responsible for the particular scattering event. Only transitions for which the product of the wave functions for the initial and final states contain a component that transforms as a symmetric second rank tensor are Raman allowed. Under 0_h symmetry the six symmetric second rank tensors transform like the A_{1g}, E_g, or F_{2g} irreducible representations. These are respectively nondegenerate, doubly degenerate, and triply degenerate. Associated with each symmetry component are appropriate forms of the polarizability tensor. These have been tabulated in Loudon[17] (corrected in Loudon[33]). In general, different scattering geometries can separate the spectra assigned to these different symmetries (although the A_{1g} component cannot be completely isolated). We have used the convention that α_{E_g} is the constant multiplying the tensors associated with E_g-like transitions and a similar meaning to $\alpha_{A_{1g}}$ and $\alpha_{F_{2g}}$. Table 4-1 has been constructed in order to illustrate how different geometries facilitate the above-mentioned separations. Note that spectra of purely E_g and F_{2g} symmetries can be obtained.

Data was taken on KCl:CN$^-$, KBr:CN$^-$, NaCl:CN$^-$, KCl:OH$^-$, and KCl:OD$^-$ and are shown in Figures 4-1 to 4-6. Figure 4-1 shows a curve of pure KCl for the normal second order spectrum and a curve for

	$\hat{E}_0$	$\hat{k}_0$	$\hat{E}_s$	$\hat{k}_s$	Intensity Proportional to
Case					
1	$\frac{1}{\sqrt{2}}(110)$	$\frac{1}{\sqrt{2}}(1\bar{1}0)$	$\frac{1}{\sqrt{2}}(\bar{1}10)$	(001)	$\lvert \alpha_{E_g} \rvert^2$
					$\frac{1}{2}(I_{xxxx} - I_{xxyy})$
2	(100)	(010)	(100)	(001)	$\lvert \alpha_{A_{1g}} \rvert^2 + \frac{4}{3}\lvert \alpha_{E_g} \rvert^2$
					I_{xxxx}
3	(010)	(100)	(100)	(001)	$\lvert \alpha_{F_{2g}} \rvert^2$
					I_{xyxy}
4	$\frac{1}{\sqrt{2}}(110)$	$\frac{1}{\sqrt{2}}(1\bar{1}0)$	$\frac{1}{\sqrt{2}}(110)$	(001)	$\lvert \alpha_{A_{1g}} \rvert^2 + \frac{1}{3}\lvert \alpha_{E_g} \rvert^2 + \lvert \alpha_{F_{2g}} \rvert^2$
					$\frac{1}{2}(I_{xxxx} + I_{xxyy} + 2I_{xyxy})$

Table 4-1: Low frequency scattering results for various geometries. $\hat{E}_0$ and $\hat{k}_0$ are unit vectors describing the directions of the polarization and propagation of the incident light, respectively, with $\hat{E}_s$ and $\hat{k}_s$ analogously defined for the scattered light. The directions of $\hat{k}_0$ and $\hat{k}_s$ are listed for convenience and do not determine scattering results.

. 3 mole % KCl:CN⁻ at room temperature having the same scattering symmetry. In general the alkali halides have a relatively large second order structure, and at $300°K$ the second order spectrum greatly obscures the possible influence of the impurity in KCl:CN⁻. There are no significant differences between the spectra, for the pure and doped crystals, shown in Figure 4-1. The gradual rise in signal as one goes to smaller shifts was a common feature to much of the data taken at room temperature. For all systems measured at room temperature there were either no effects that could be correlated with the presence of impurities or a structureless rise in intensity as in KCl:CN⁻. This may be due to two possible effects. Either the second order spectrum is too large and really masks the impurity induced structure or the impurity induced scattering has been temperature broadened. Both of these effects are significantly reduced in the spectra taken from samples that were at helium temperatures. In fact in many samples the second order scattering is largely frozen out at low temperatures.

In Figure 4-2 the normal second order spectrum for only symmetry combination (the largest contribution) of pure KCl and the three Raman active scattering geometries are presented for . 53% KCl:CN⁻ at helium temperatures. In the doped samples arrows have been used to indicate second order structure. There is a significant impurity induced structure, and it should be noted that there are spectra corresponding to all of the possible Raman active symmetries and they all have comparable intensities.
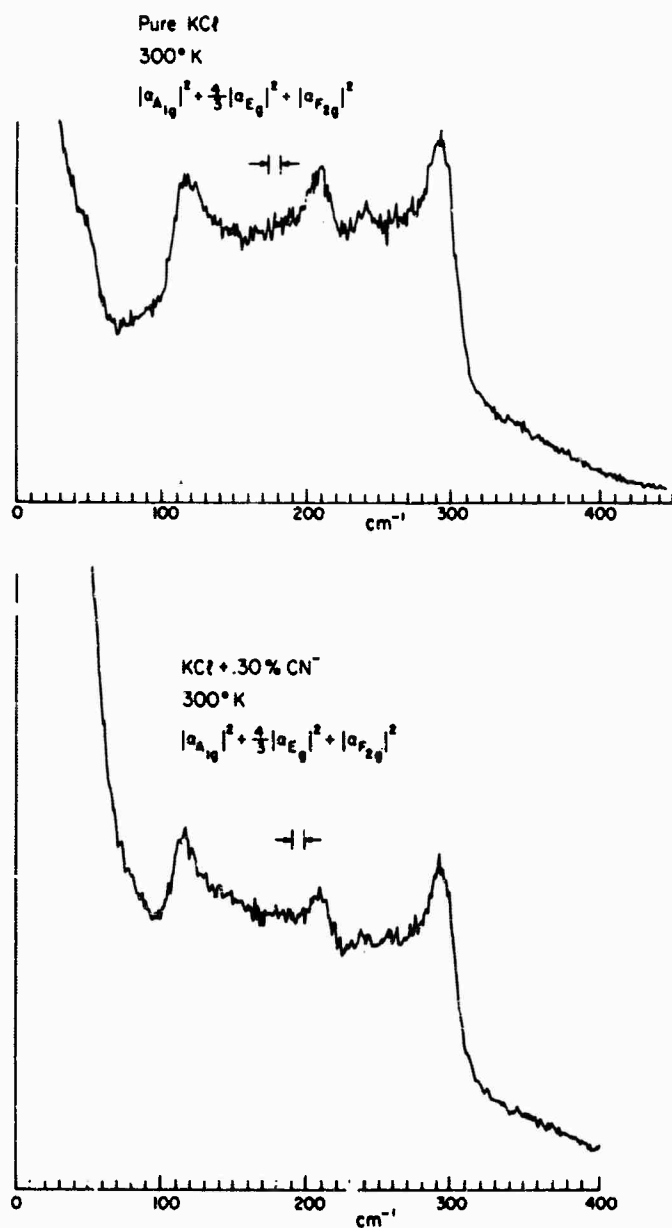
Pure KCl
300° K
$|a_{A_{1g}}|^2 + \frac{4}{3}|a_{E_g}|^2 + |a_{F_{2g}}|^2$

KCl + .30 % CN⁻
300° K
$|a_{A_{1g}}|^2 + \frac{4}{3}|a_{E_g}|^2 + |a_{F_{2g}}|^2$

Fig. 4-1 Room temperature low frequency data for KCl and KCl:CN⁻.
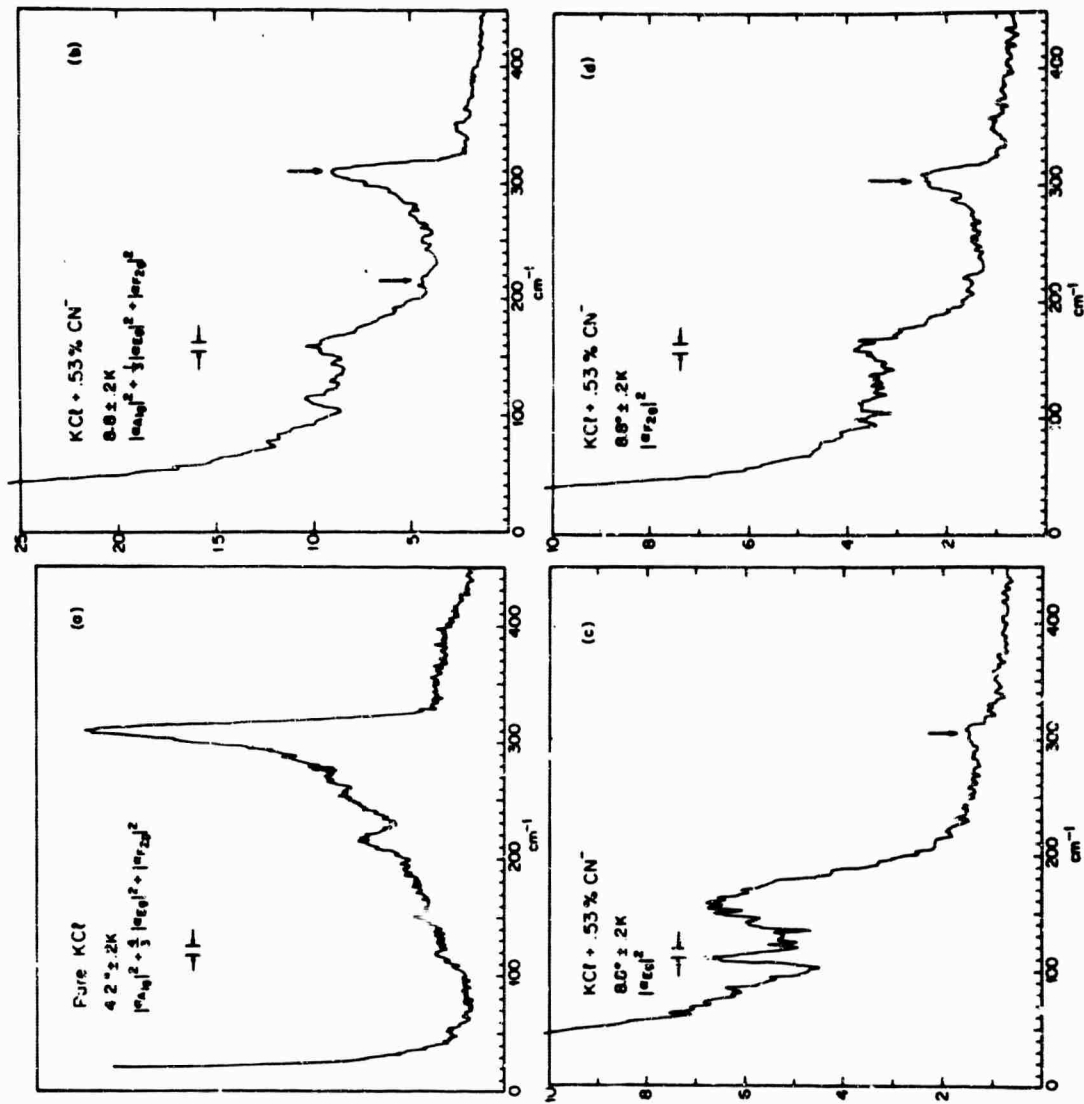
Fig. 4-2 Helium temperature low frequency data for KCl and KCl:CN⁻.

In Figure 4-3 results are given for 0.72% KBr:CN$^-$. In Fig. 4-3a the KBr second order spectrum is shown for the symmetry that produces the strongest scattering. In Fig. 4-3b the spectrum corresponding to dominant impurity induced Raman scattering symmetry and a theoretical curve discussed in section IV. B. are given. For this symmetry the contribution to the signal from the second order spectrum is very small and is estimated to be less than 5% of the signal in 4-3b. For this system the other two symmetry components to the impurity scattering were observed to be small compared to the $|\alpha_{E_g}|^2$ component. Since the second order spectrum for the other two components is quite large, it was difficult to estimate the relative magnitudes of the various impurity induced spectra. However, the $|\alpha_{E_g}|^2$ impurity spectra is about a factor of 5 to 10 larger than components due to $|\alpha_{A_{1g}}|^2$ or $|\alpha_{F_{2g}}|^2$.

Figure 4-4 contains the data for NaCl and .63% NaCl:CN$^-$. In this case it was found that the impurity contribution due to $|\alpha_{E_g}|^2$ was negligible compared with the other two components. It is found, then, that all three of the CN$^-$ doped hosts give very different results, both in regard to the symmetry designation of the spectra and in the shape and general character of the results.

For the purposes of illustration and because it offers a chance of qualitative comparison for difference impurities in the same host, data for 1.2% KCl:OH$^-$ and .4% KCl:OD$^-$ are shown in Figures 4-5 and 4-6. Data which would separate the $|\alpha_{A_{1g}}|^2$ and $|\alpha_{E_g}|^2$ components were not taken for KCl:OH$^-$.
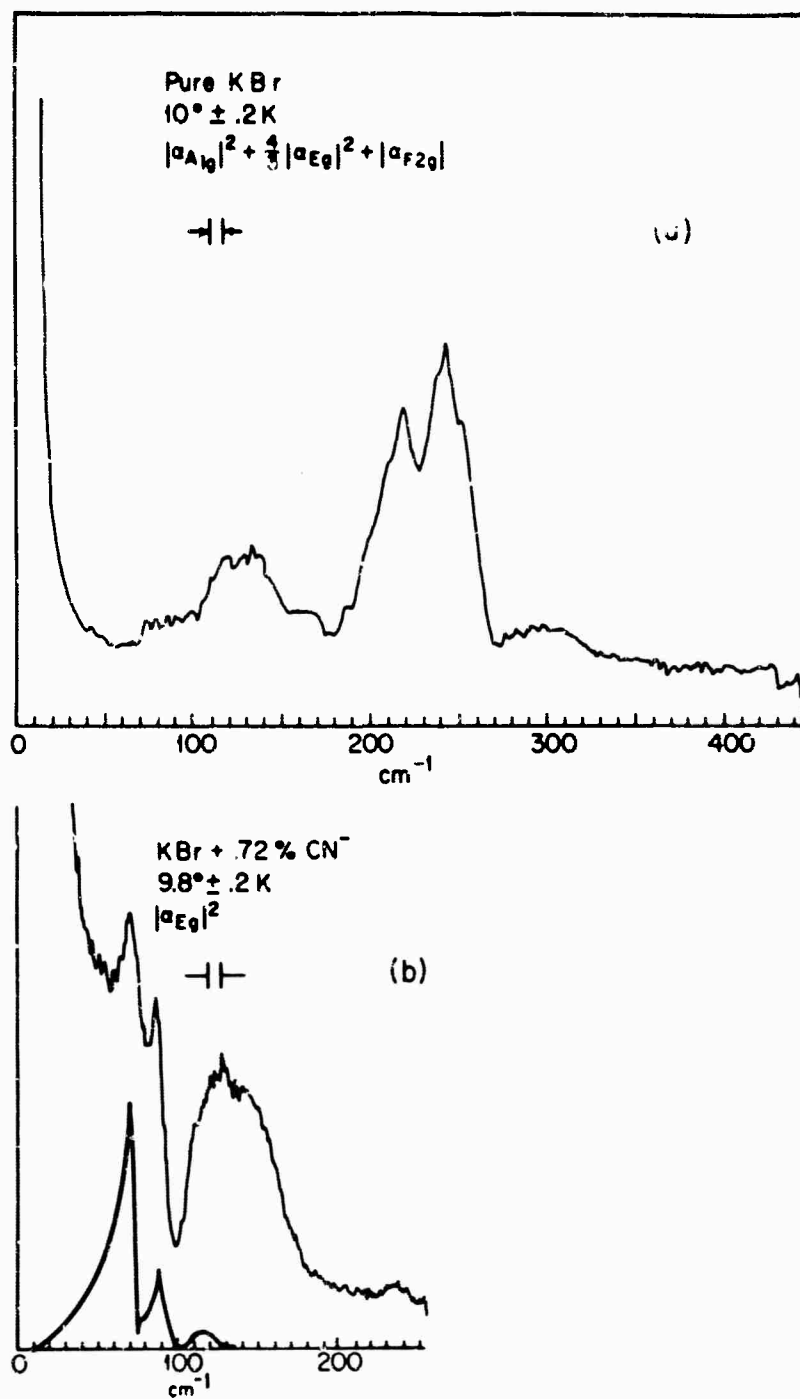
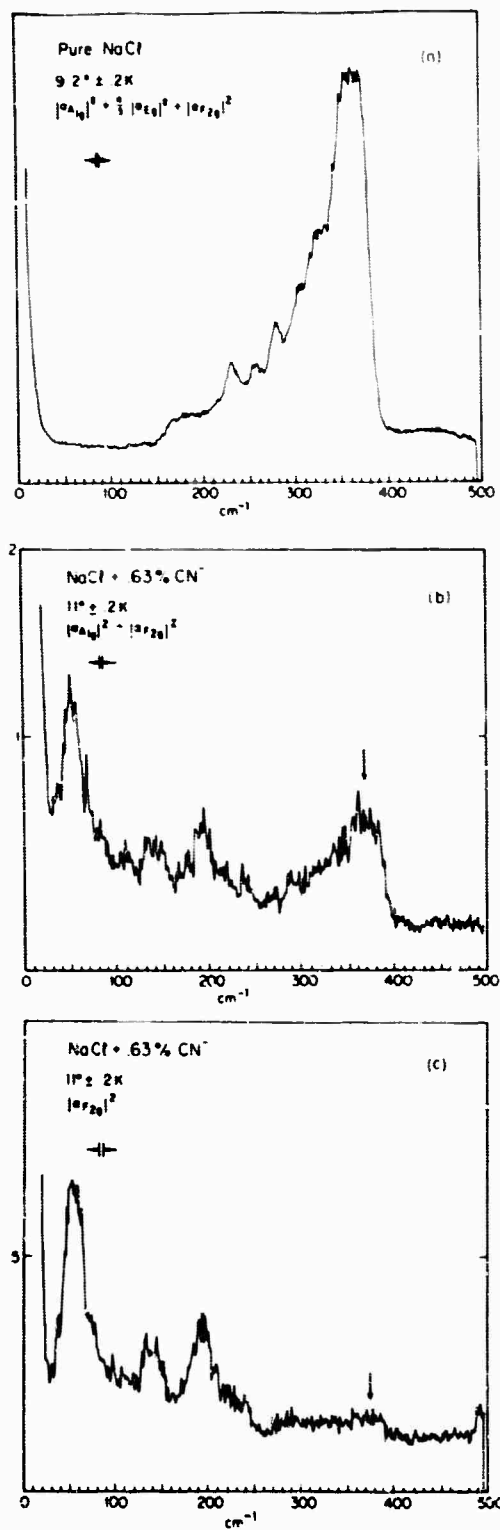Fig. 4-3 Helium temperature low frequency data for KBr and KBr:CN⁻.

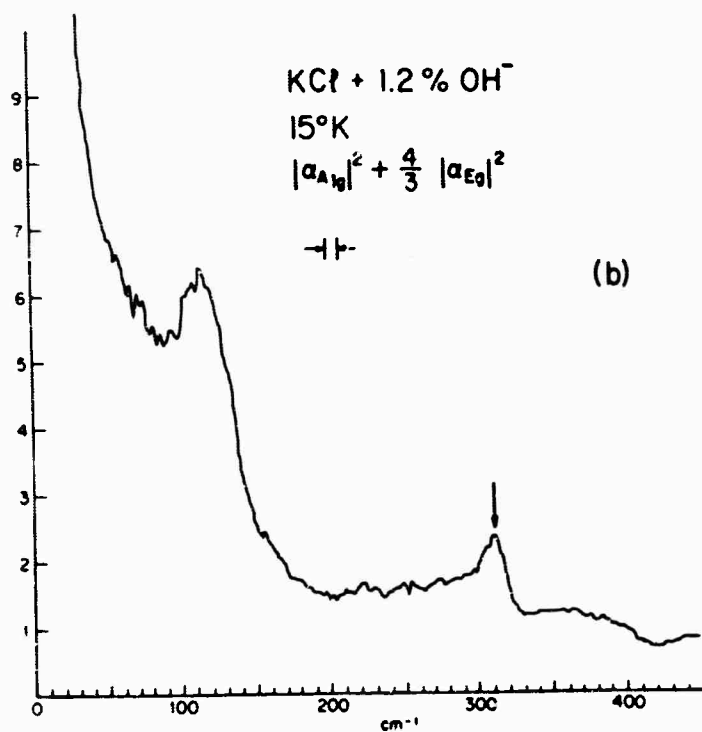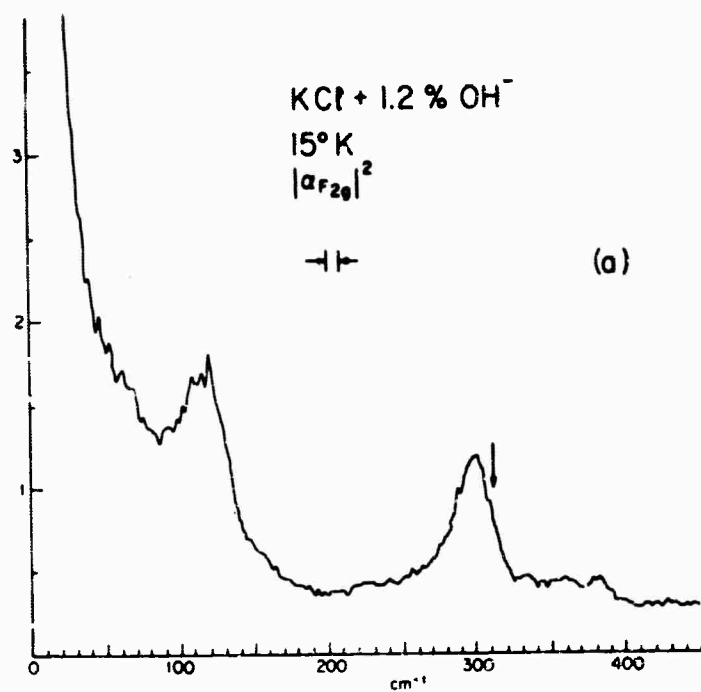Fig. 4-4 Helium temperature low frequency data for NaCl and
NaCl:CN⁻.

KCl + 1.2 % OH⁻
15° K
$|\alpha_{F_{2g}}|^2$

(a)

KCl + 1.2 % OH⁻
15°K
$|\alpha_{A_{1g}}|^2 + \frac{4}{3} |\alpha_{E_g}|^2$

(b)

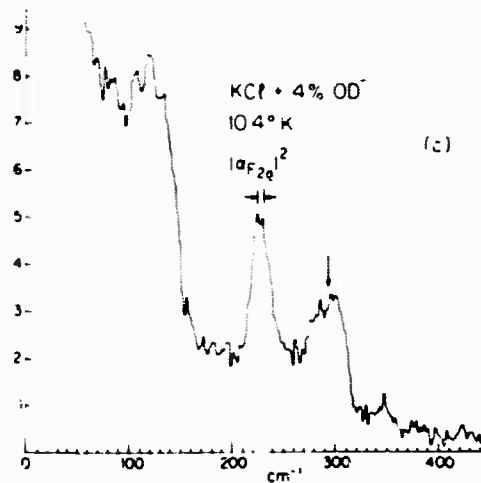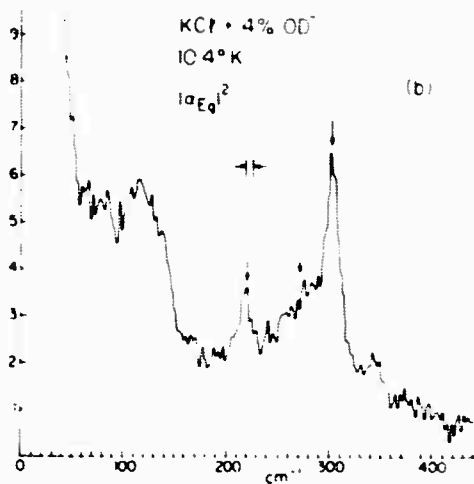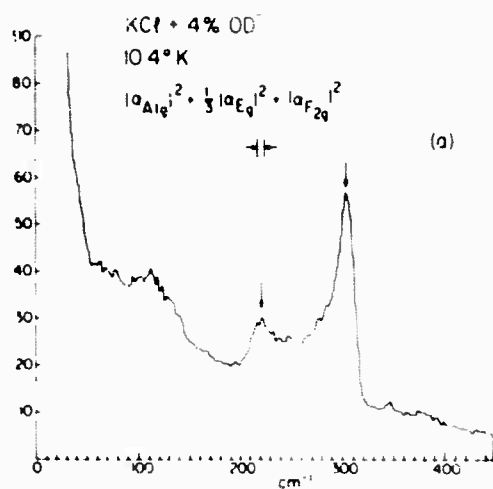Fig. 4-5 Helium temperature low frequency data for KCl:OH⁻.

Fig. 4-6 Helium temperature low frequency data for KCl:OD⁻.

B. Discussion

It is quite instructive to begin the discussion of the low frequency Raman scattering results with the spectra of Figure 4-3 for the KBr:CN⁻ system. For KBr:CN⁻, the infrared work reported by Seward[2] and the conclusions that are to be drawn in section V of this paper indicate that CN⁻ molecule is not very heavily trapped in the sense that it is relatively free to rotate.

Assuming that for a zeroth approximation one may regard the impurity as though it were a spherical ion which simply changes the mass and force constants of the ion it has replaced. For this type of problem there have been a number of theoretical treatments including Benekek and Nardelli[22] and Xinh[18] who consider Raman scattering from alkali halides doped with atomic impurities. The most recent results, however, are these of Harley, Page and Walker[23] who studied T_ℓ^+ doped potassium halides. Although they have a great deal of experimental results with which one might profitably compare the results presented here we only wish to make use of their theoretical results.

Employing what has now become standard Green's function methods[19] Harley et al[23] calculated the spectrum for Raman scattering induced by the presence of T_ℓ^+ impurities in potasium halides. In particular, similar to the data given above, there are different spectra for A_{1g}, E_g, T_{2g} experimental symmetries. Figure 4-3b shows both the experimental spectra for E_g symmetry as observed for scattering from CN⁻ doped KBr and the theoretical spectrum calculated by Harley et al.[23] From Figure 2 of reference 23 one can see

there is also excellent agreement between the E_g Raman spectrum induced in KBr by T_ℓ^+ impurities and this theoretical spectrum.

The similarities between these different spectra a quite striking evidence that for the CN⁻ impurity in KBr the low frequency part of the impurity induced spectra can be largely explained by the same mechanisms that serve to explain the Raman scattering induced by spherica'ly symmetric impurities. Similar conclusions can be drawn for the other potassium salts with CN⁻ impurities.

The main difference in the two curves in Figure 4-3b is the gradual structureless rise in the KBr:CN⁻ data as ω approaches zero. As it is structureless, it is very difficult to assign its origin. It may well be due, in part at least, to the rotational motion of the molecule. In the results of section V, there is a sideband, with a sharp peak that is shifted from the stretching vibrational mode by 13 cm⁻¹ and extending to 30 cm⁻¹ or so. This band should appear in the low frequency data for the reasons discussed in section II. That is that the change induced in the polari.ability tensor by the stretching mode has exactly the same symmetry as the static polarizability tensor for the rigid molecule. The sharp peak itself may be masked by spurious laser leakage through the spectrometer (the optical quality of this crystal made scans near 13 cm⁻¹ quite difficult), but the gradual rise could be due to the tail of this line.

The results for NaCl:CN⁻ as contained in Figure 4-4 are much more difficult to interpret than KCl:CN⁻ or KBr:CN⁻. Here, as will be discussed in section V, the CN⁻ molecule is rather heavily trapped in the NaCl lattice in the sense that it is not free to rotate. A careful

analysis taking into account the changes in force constants due to the impurity and its molecular motion is needed. Roughly, however one can obtain some information in the following manner. Benedek and Nardelli[22] showed that to a very good approximation, if $I_\Gamma(\omega)$ describe the spectrum, associated with a particular symmetry Γ, of the first order Raman scattering induced by a spherical impurity than for Stokes radiation

$$I_\Gamma(\omega) \sim \frac{(N(\omega) + 1)}{\omega} \rho_\Gamma(\omega)$$

where $N(\omega)$ is the Bose-Einstein thermal factor (i. e. $N(\omega) = [e^{\hbar\omega/kT} - 1]^{-1}$), ω is the frequency shift from the laser frequency, and $\rho_\Gamma(\omega)$ represents the phonon density of states of the impure crystal projected along the Γ symmetry. Now to first order $\rho^0_\Gamma(\omega)$, the density of states of the pure crystal, may be compared to $\rho_\Gamma(\omega)$. This is very similar to the calculation of Harley et al[23] mentioned above. In fact if one uses Timusk and Klein's[34] calculated density of states $\rho^0_{E_g}(\omega)$ rough agreement is also obtained with the spectra in Figure 4-3.

Timusk's calculations[35] for pure NaCl show peaks in the total density of states at about 120 cm^{-1}, 140 cm^{-1}, and 180 cm^{-1}. Except for the line centered at 54 cm^{-1} in Figures 4-4b and 4-4c, these peaks are in rough agreement with the results of NaCl:CN$^-$. When the total density of states is projected along the appropriate symmetry components, there is no longer any real agreement. The line at 54 cm^{-1}, which seems to be almost completely F_{2_g} symmetry is probably due to the rotational motion of the molecule as it is repeated in the sideband results of section V with the same scattering symmetry.

The KCl:OH⁻ and KCl:OD⁻ cases in Figures 4-5 and 4-6 may be compared to each other and to KCl:CN⁻. The lines at 300 cm^{-1} in KCl:OH⁻ and 228 cm^{-1} in KCl:OD⁻, having apparently only F_{2_g} symmetry, are probably associated with molecular motion of the respective molecules. They have been seen as sidebands to the stretching modes in infrared absorption. The values for the I.R. experiment are 298 cm^{-1} and 232 cm^{-1} respectively for OH⁻ and OD⁻.[7] Recently Klein et al[36] have attempted to explain this line as arising from torsional harmonic oscillations of the hydroxyl molecule. The principal basis for this model is the observation of the OH⁻/OD⁻ isotope shift in frequency. The measured shift is relatively well explained by a torsional harmonic oscillation model. The 300 cm^{-1} line in KCl:OH⁻ has been previously seen by Raman measurements by Fenner.[37] Here the line was reported at 305 cm^{-1} having only F_{2_g} symmetry in agreement with our results. This scattering symmetry supports the conclusion that the hydroxyl motion in this case is due to a relatively small angle torsional oscillation.[37] The structure at 110 cm^{-1} for both symmetries and in both NCl:OH⁻ and KCl:OD⁻ is probably due to modified phonon structure scattering as it neither shifts with the isotope used and compares roughly to the scattering found in KCl:CN⁻.

To conclude, the impurity induced scattering effects can be correlated to a mixture of impurity induced phonon scattering and molecular rotational scattering. Both of these effects are comparable for the cases studied here and cannot be really isolated using just the information from the Raman scattering. In fact they may not be theoretically isolated.

V.   High Frequency Results

   A.   Trace Scattering

As discussed in connection with Eq. (2-15), the high frequency spectra is expected to be composed of a very narrow trace component and sideband structure centered at the frequencies of the internal modes of the molecule. This type of scattering behavior was observed. Table 5-1 summarizes the data we have taken as to position and half width of the trace scattering for various impurities and hosts. There are several features that should be noted. First, the trace components are very narrow, even at room temperature, and exhibit only small changes in width and position as the temperature is lowered from $300^{\circ}K$ to helium temperatures. Defining a Q-factor in the usual way as $\omega/\Delta\omega$, $Q \gtrsim 2000$ for the CN^- doped samples and $Q \sim 100$ or better for the others. Second, with the possible exception of the OH^- doped systems at elevated temperatures, the position of the trace scattering agrees to within experimental error with the supposed "Q(0)" position measured by infrared absorption on the same impurity host system. The possible discrepancy in the case of the OH^- systems may be due to the fact that, in the higher temperature regions, the I. R. results are quite broad in these samples, and the Q(0) position is not easily determined. The position of the trace scattering for the $KCl:OH^-$ system as determined by Fenner and Klein[37] is in agreement with ours. The room temperature value of the I. R. Q(0) position of $KCl:OD^-$ has not been reported. As a third observation, we found the B_1 mode for both $KCl:NO_2^-$ and $KBr:NO_2^-$ at room temperature to be very broad. For this reason, the frequency of this internal mode at

room temperature is not given in Table 5-1. We have in this case,

quite simply, that $Tr \underset{\sim}{\alpha}^{B_1}(MF) = 0$, and there are no components in

the Raman spectrum except those broadened by the rotational motion.
We will return to this important point later in this section.

The temperature dependence of the linewidth of the trace component for .54% CN^-:KCl has been plotted in Figure 5-1. We also performed measurements on the KCl:OH^- system and found a more or less linear change in linewidth with temperature (from $300^{\circ}K$ to $10^{\circ}K$) in agreement with previous measurements of Fenner and Klein.[37] The interpretation of these effects is quite difficult as it is necessary to know the details of the interaction between host and molecule as well as the rotational motion of the molecule. In general, these linewidths are small and we believe them to be of only second order importance. We do not try to interpret them here.

As a further consistency check for the formulism of section II, it is interesting to examine the KBr:NO_2^- system. Here the molecule has two stretching modes which have a predicted trace scattering and one mode, the antisymmetric B_1 normal vibration, which as mentioned above, does not. The Raman spectra attributed to one of the A_1 modes and to the B_1 mode of this system is pictured in Figure 5-2 for a particular scattering symmetry. It is apparent the A_1 mode has a large central component at all temperatures due to the $\bar{\alpha}^\nu$ component, but at $200^{\circ}K$ the B_1 mode is barely visible as a broad band. As the temperature is lowered, it becomes better and better defined as the rotational motion is frozen out. At $15^{\circ}K$, we made careful measurements on the relative intensities of the three Raman active components for these two modes.

Dopant	Host		Trace Position (cm^{-1})	Half Width (cm^{-1})
CN^-	KCl		2084.4	.9
	KCl	(8.5^oK)	2087.1	.4
	KBr		2075.4	~1.0
	KBr	(9^oK)	2077.5	<.6
	NaCl		2102.4	.85
	NaCl	(10^oK)	2106.2	.4
	RbCl		2077.1	<1
	RbBr		2068.4	<i. ऽ
OH^-	KCl		3628	6.5
	KCl	(10^oK)	3642	<.8
	KBr		3598	<.5
OD^-	KCl		2677	<5.0
	KCl	(10^oK)	2685	<1.0
NO_2^-	KCl		1323 (A_1)	~3
			806 (A_1)	<4
	KBr		1317 (A_1)	~10
			805 (A_1)	~3

Table 5-1: Raman data for the trace scattering of different impurity host combinations. Except where noted, all data is at 300^oK.
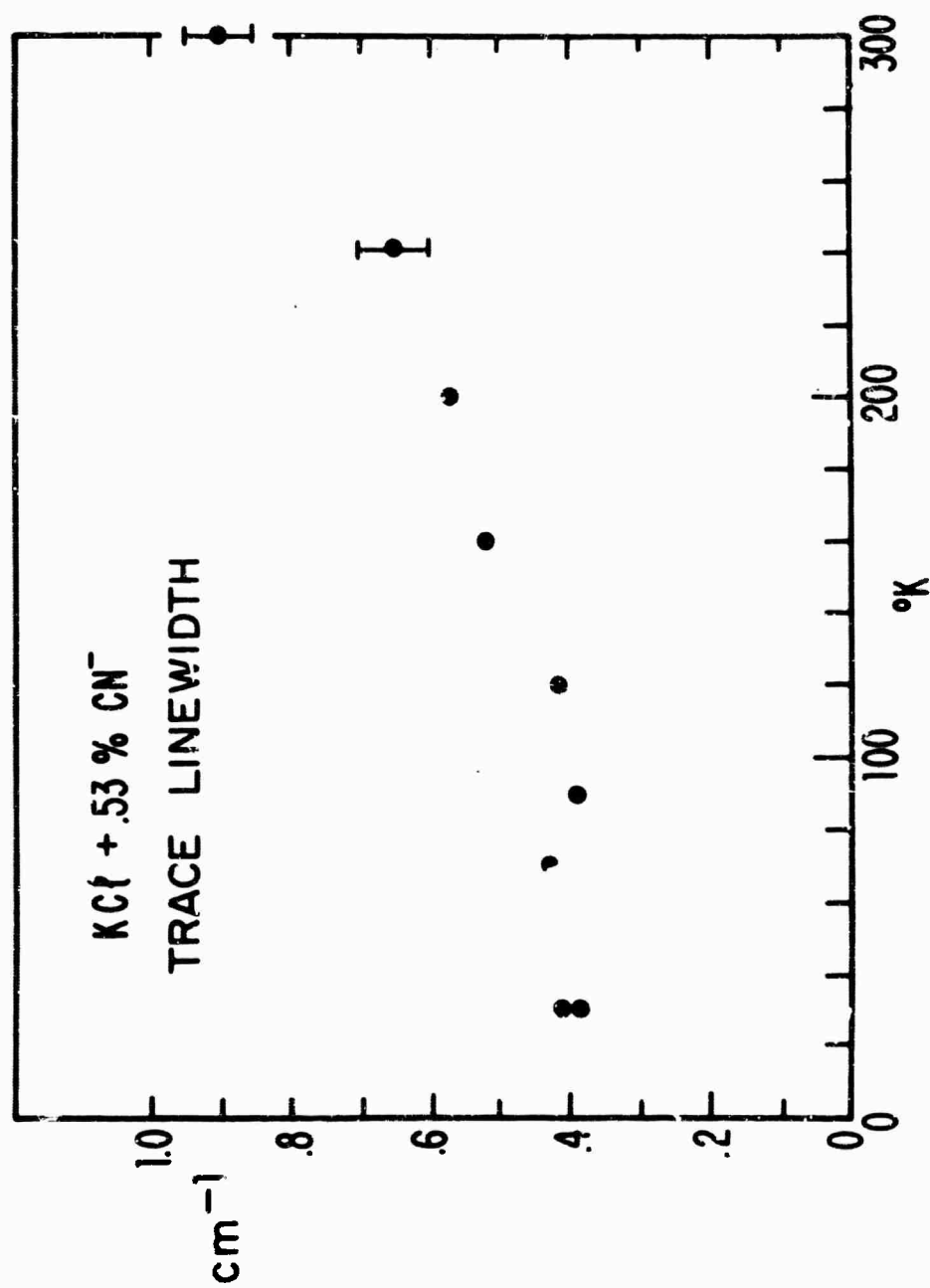
Fig. 5-1 Linewidth of KCl:CN⁻ trace scattering as a function of temperature.

KBr +.15 % NO$_2^-$

$(\bar{a}^\nu)^2 + \langle \beta_{xx}^\nu(t)\, \beta_{xx}^\nu(o)\rangle$
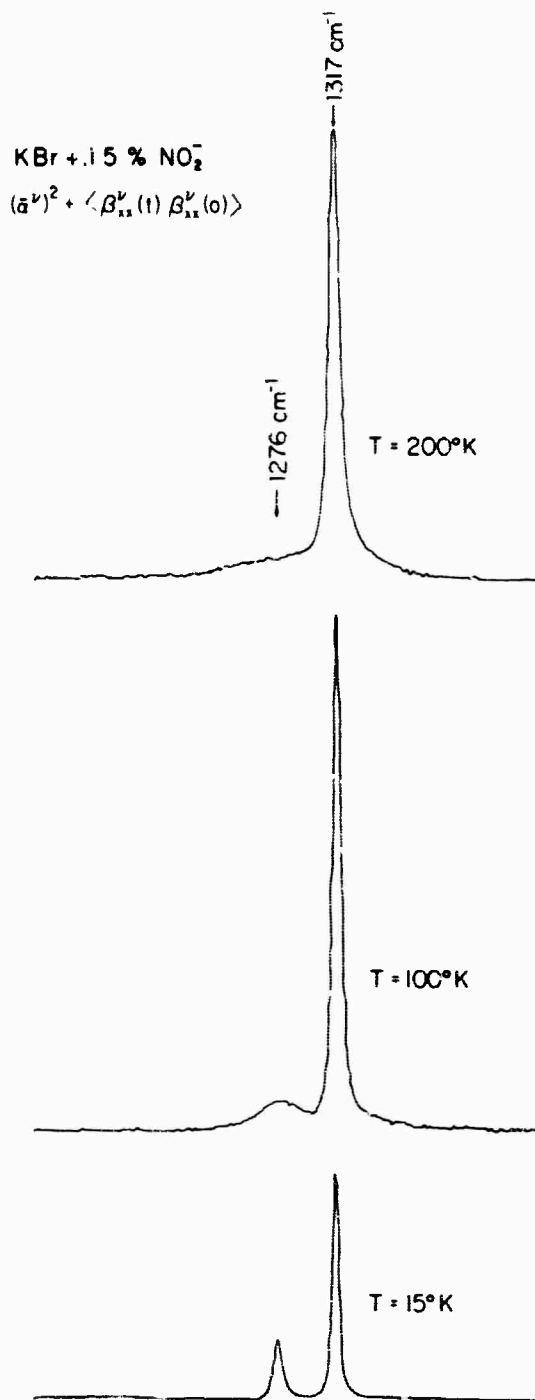
1317 cm^{-1}

1276 cm^{-1}

T = 200°K

T = 100°K

T = 15°K

Fig. 5-2 High frequency data at various temperature of KBr:NO$_2^-$ in the vicinity of one A$_L$ (1317 cm^{-1}) internal mode and the B$_1$ (1276 cm^{-1}) internal mode.

The results are given in Table 5-2 for the integrated intensities. Consistent with the theoretical framework the B_1 mode has no $(\overline{\alpha}^\nu)^2$ component whereas the A_1 mode has a large $(\overline{\alpha}^\nu)^2$ component.

B. Sideband Data

Results at selected temperatures are given in Figures 5-3 and 5-4 for .54 mole % CN⁻ in KCl and .72% KBr:CN⁻ respectively. For these two cases and all others reported in this section, the trace position for a particular temperature is taken as the origin of the frequency scale. The data are very similar for both systems. At the higher temperature, the two scattering symmetries look very much alike: a reasonably well-defined peak on each side of the trace position. As the temperature is lowered, the peaks in the $\langle \beta^\nu_{xx}(t)\beta^\nu_{xx}(0)\rangle$ polarization remain well defined (except for the freezing out of the low energy side due to the Boltzmann factor). At helium temperatures for this polarization, there is one line shifted to the high energy side by 13 cm⁻¹ and 16 cm⁻¹ for KBr:CN⁻ and KCl:CN⁻ respectively. However, as the temperature is lowered, the $\langle \beta^\nu_{xy}(t)\beta^\nu_{xy}(0)\rangle$ component for these samples ceases to have really well-defined peak structure at approximately 80°K in KBr:CN⁻ and 120°K in KCl:CN⁻.

Both samples also show significant resolution limited scattering at the trace position. Some of this may be real as we shall discuss later, but some may also be due to experimental uncertainties. The trace scattering is very large and it is difficult to completely eliminate it from the signal. As a practical matter, the polaroid sheet after the sample is rotated until a minimum is reached in the intensity of the trace scattering. However, as the signals are weak in these sideband

$$(\bar{\alpha}^{\nu})^2 \; : \; \langle \beta^{\nu}_{xx}(t)\beta^{\nu}_{xx}(0)\rangle \; : \; \langle \beta^{\nu}_{xy}(t)\beta^{\nu}_{xy}(0)\rangle$$

	$(\bar{\alpha}^{\nu})^2$		$\langle \beta^{\nu}_{xx}(t)\beta^{\nu}_{xx}(0)\rangle$		$\langle \beta^{\nu}_{xy}(t)\beta^{\nu}_{xy}(0)\rangle$
$\nu^{B_1}_{(1276)}$	$.08 \pm .15$	:	1	:	.34
$\nu^{A_1}_{(1317)}$	4.6	:	1	:	3.27

Table 5-2: Relative integrated intensities for the three independent spectral components of two of the NO_2^- modes at $15\,^\circ K$. The $\langle \beta^{\nu}_{xx}(t)\beta^{\nu}_{xx}(0)\rangle$ intensity is taken as unity for both the B_1 and A_1 modes.

KCl + .53% CN⁻

$\langle \beta'_{xy}(t)\,\beta'_{xy}(o)\rangle$

$3/4 \langle \beta'_{xx}(t)\,\beta'_{xx}(o)\rangle$

T = 280°K
⊣⊢

T = 300°K
⊣⊢

T = 230°K
⊣⊢

T = 196°K
⊣⊢

T = 200°K
⊣⊢

T = 101°K
⊣⊢

T = 140°K
⊣⊢

T = 60°K
⊣⊢

T = 120°K
⊣⊢

T = 40°K
⊣⊢

T = 80°K
⊣⊢

15.9

T = 20°K
⊣⊢

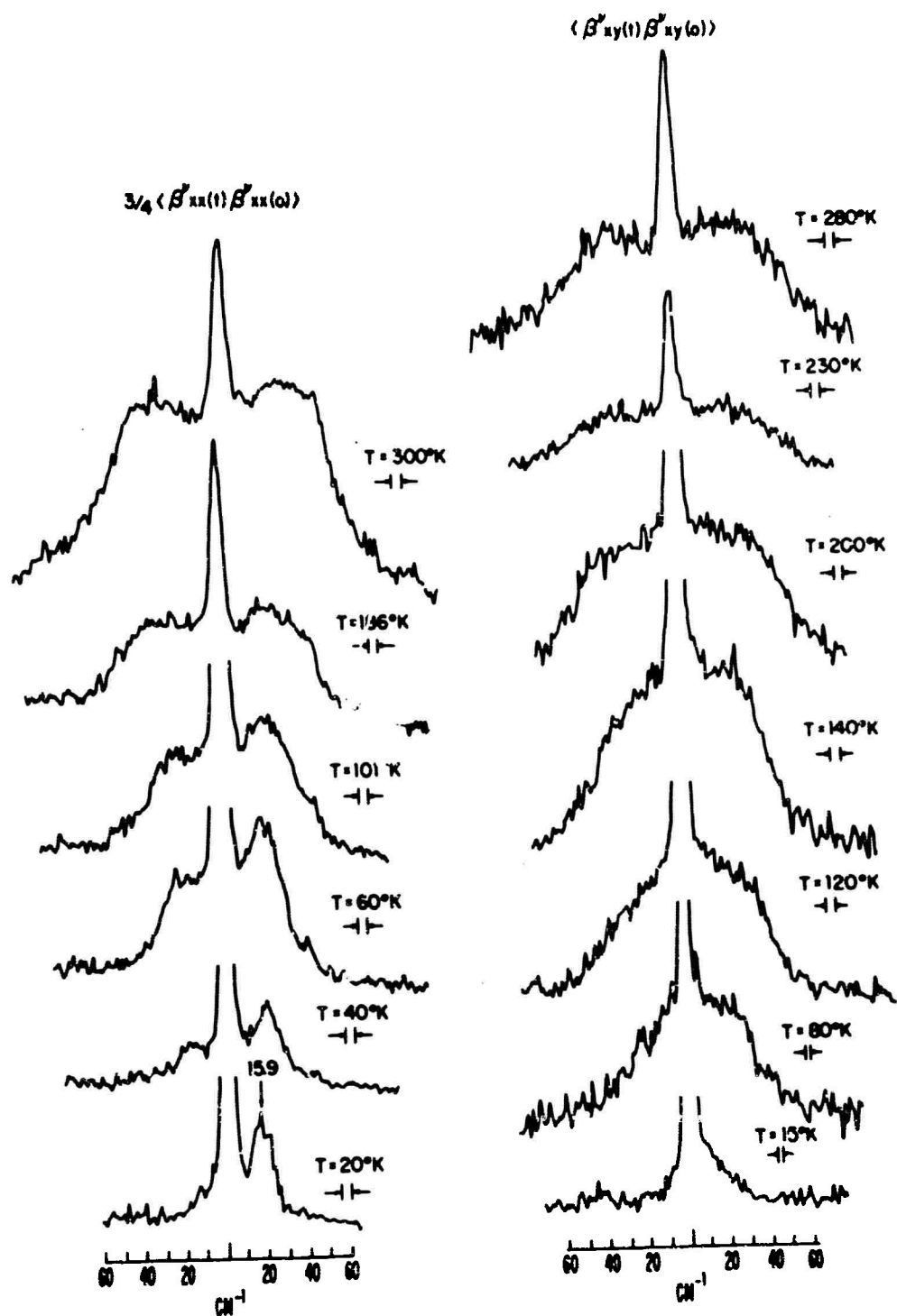T = 15°K
⊣⊢

60 40 20   20 40 60
CM⁻¹

60 40 20   20 40 60
CM⁻¹

Fig. 5-3 High frequency sideband data for KCl:CN⁻. Stokes shifts are to the right.
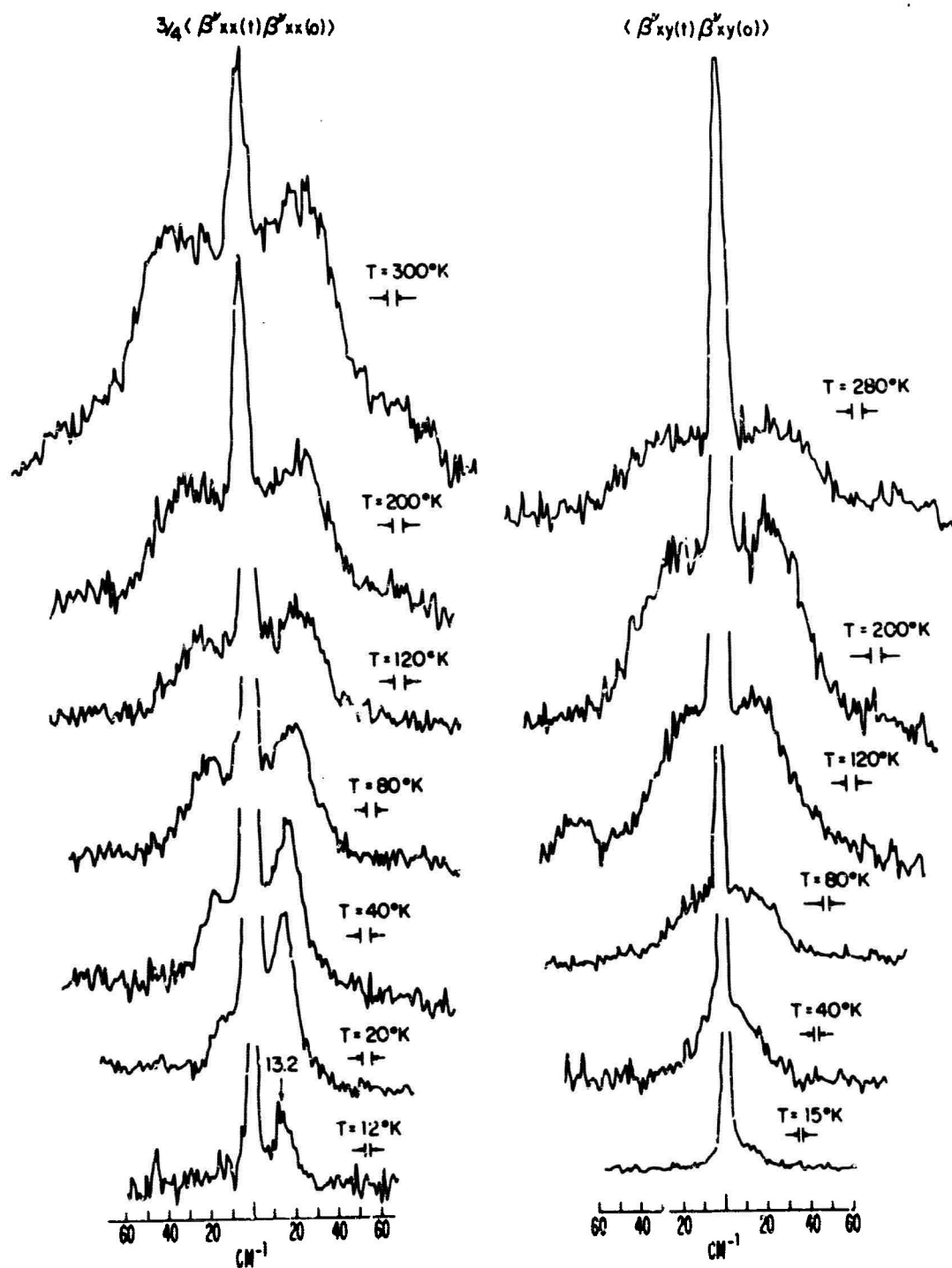
Fig. 5-4 High frequency sideband data for KBr:CN⁻. Stokes
shifts are to the right.

spectra, occasionally some trace scattering may not be eliminated. A second, but more formidable experimental problem, is the fact that by focusing the laser in the sample, to some extent the laser beam has components for which the E-field is polarized parallel to what is nominally the average propagation direction for the incident laser beam. Using a laser beam with a diameter of .2 cm and a focusing lens of 8 cm focal length, a simple calculation shows that about one percent of the light is polarized in this way and allows spurious trace scattering that is transmitted through the polaroid analyzer. This could not be eliminated in our measurements and must be taken into account whenever signals with the $Q(0)$ frequency are analyzed.

In Figure 5-5 the . sults for .63% $NaCl:CN^-$ are given. The $\langle \beta^V_{xy}(t)\beta^V_{xy}(0)\rangle$ component has a single line which shifts slightly with temperature, but is about 54 cm^{-1} from the trace frequency. In the $\langle \beta^V_{xx}(t)\beta^V_{xx}(0)\rangle$ symmetry, we see a Lorentzian line whose linewidth is temperature dependent. This linewidth is plotted as a function of temperature in Figure 5-6. To determine the linewidth, it was necessary to subtract out a small amount of trace scattering in the data which was narrower than the instrumental resolution and is probably due to the instrumental causes discussed above. The error bars in Figure 5-6 were determined by successively fitting Lorentzians to the data until the calculated curves would no longer fit the "wings" of the results.

In Figures 5-7 and 5-8 the scattering data for 1.2% $KCl:OH^-$ and .4% $KCl:OD^-$ are plotted. These two systems exhibit the same type of scattering behavior. At higher temperatures, the spectra for both

NaCl + .63% CN⁻

$3/4 \langle \beta_{xx}^{\nu}(t) \beta_{xx}^{\nu}(0) \rangle$

$\langle \beta_{xy}^{\nu}(t) \beta_{xy}^{\nu}(0) \rangle$

T=300°K
⊥

T=254°K
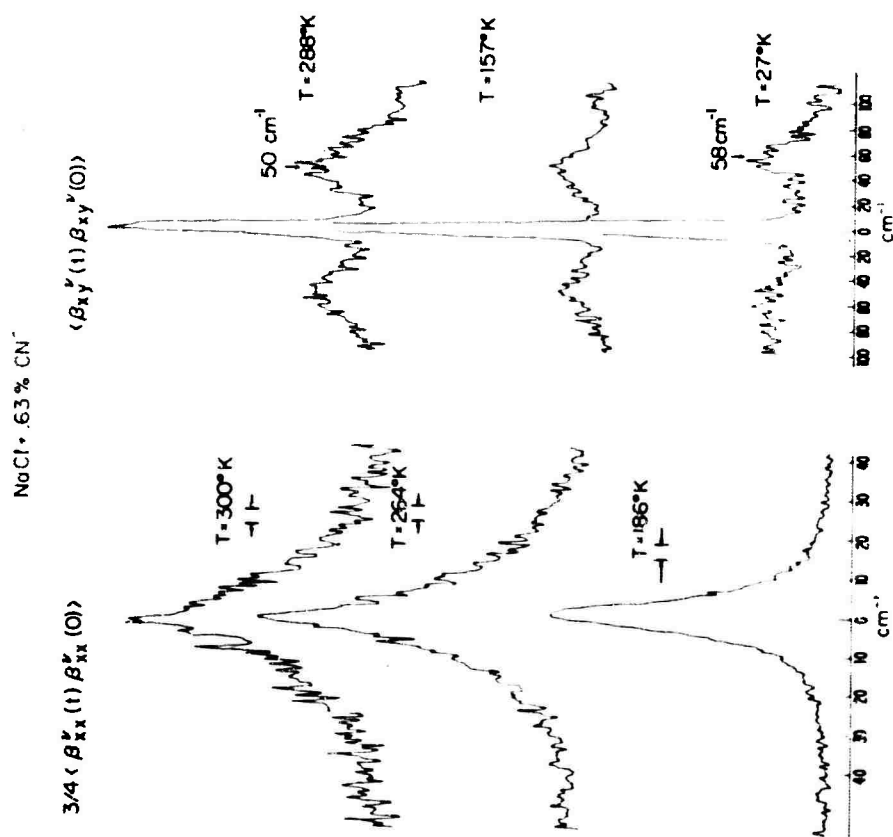⊥

T=186°K
⊥

cm⁻¹

50 cm⁻¹
T=288°K

T=157°K

58 cm⁻¹
T=27°K

cm⁻¹

Fig. 5-5 High frequency sideband data for NaCl:CN⁻. Stokes shifts are to the right.
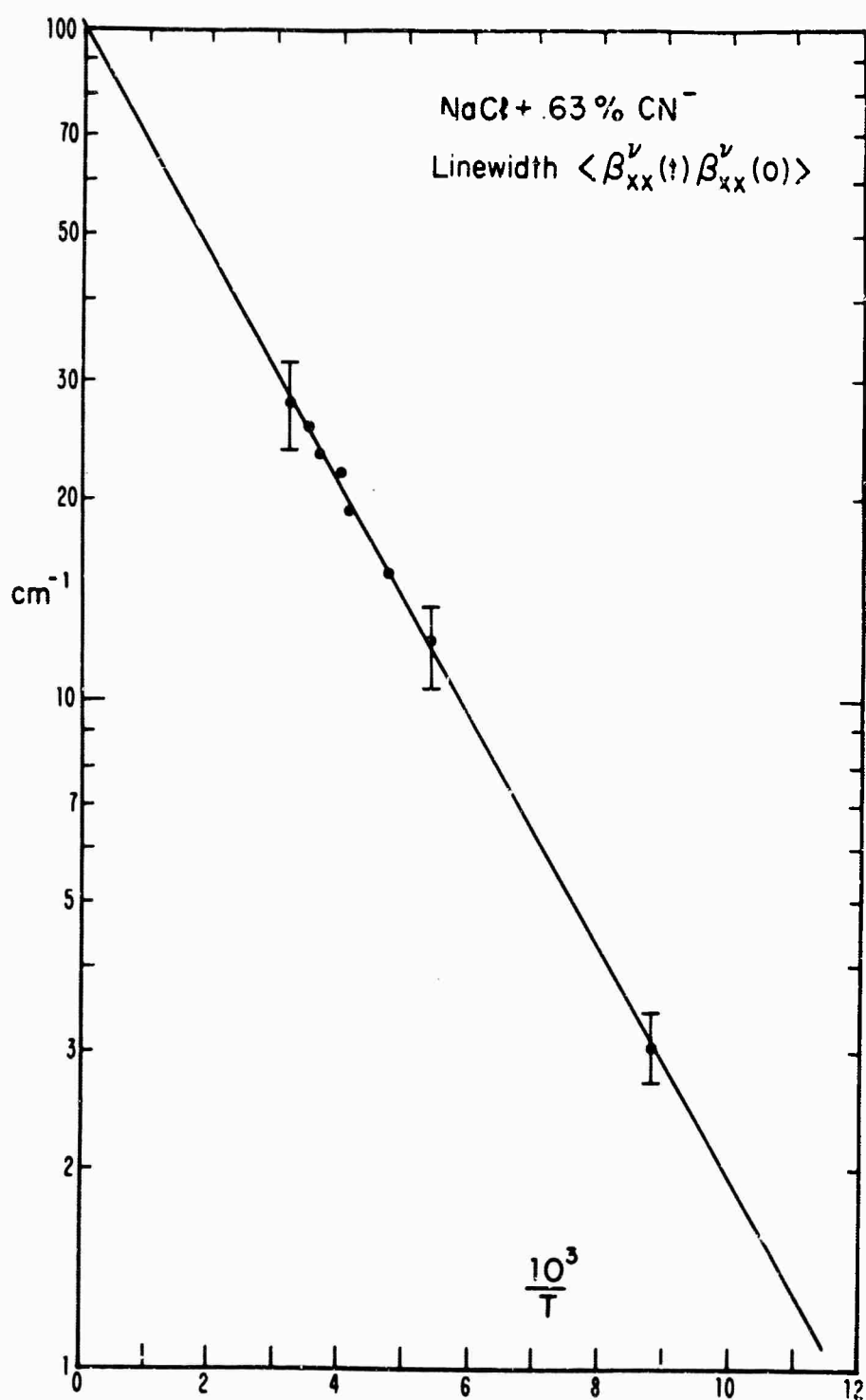
Fig. 5-6 Full width at half intensity of $\langle \beta^{\nu}_{xx}(t)\beta^{\nu}_{xx}(0)\rangle$ component for NaCl:CN$^-$ as a function of temperature.
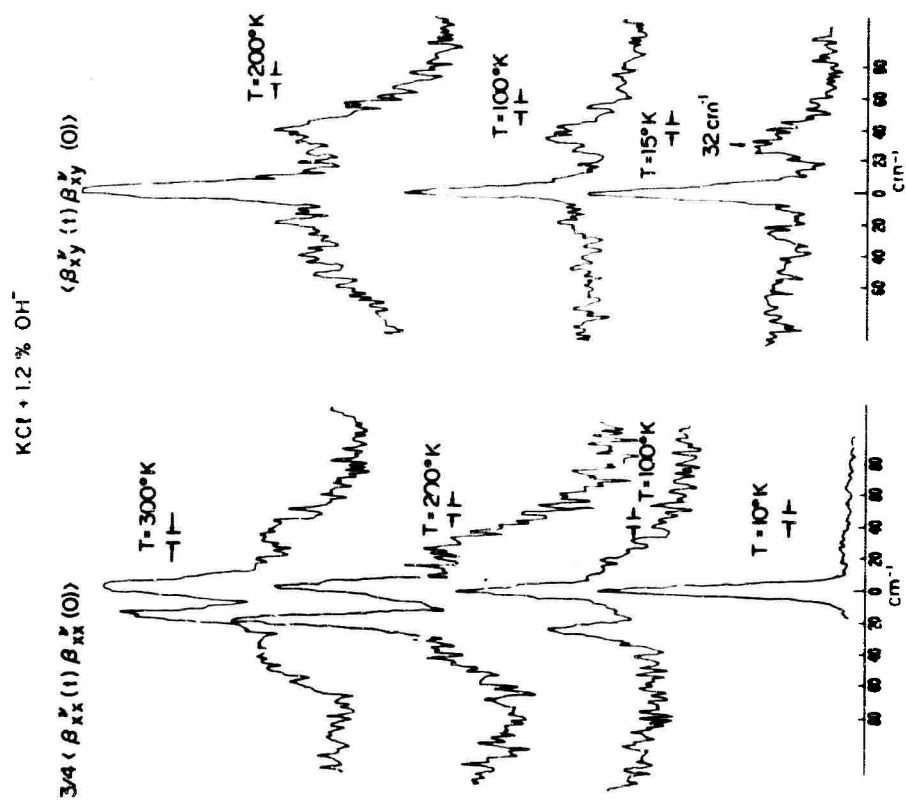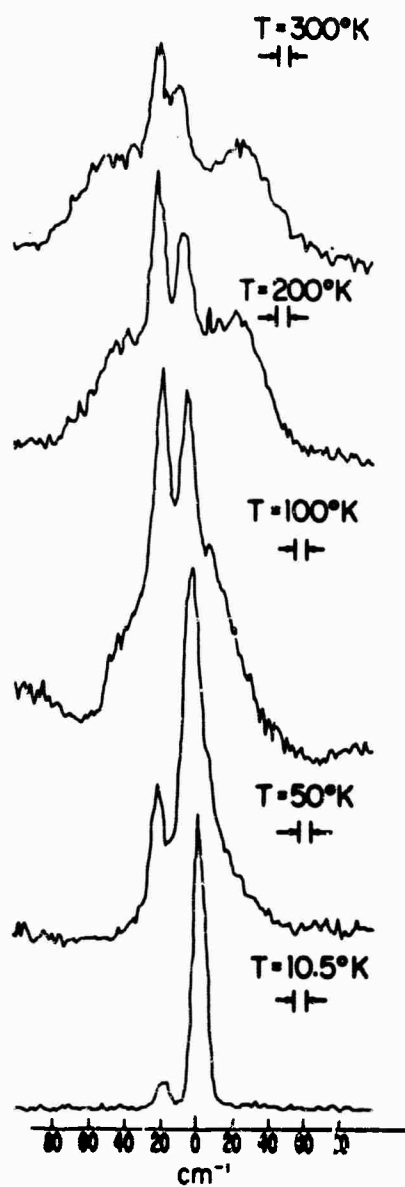
Fig. 5-7 High frequency sideband data for KCl:OH⁻. Stokes shifts are to the right.

KCl + 4% OD⁻

$3/4 \langle \beta_{xx}^{v}(t) \beta_{xx}^{v}(0) \rangle$ $\langle \beta_{xy}^{v}(t) \beta_{xy}^{v}(0) \rangle$

T=300°K
⊣⊢

T=300°K
⊣⊢

T=200°K
⊣⊢

T=200°K
⊣⊢

T=100°K
⊣⊢

T=100°K
⊣⊢

T=50°K
⊣⊢

T=10.5°K
⊣⊢

T=10.5°K
⊣⊢

25cm⁻¹

80 60 40 20 0 20 40 60 80   80 60 40 20 0 20 40 60 80
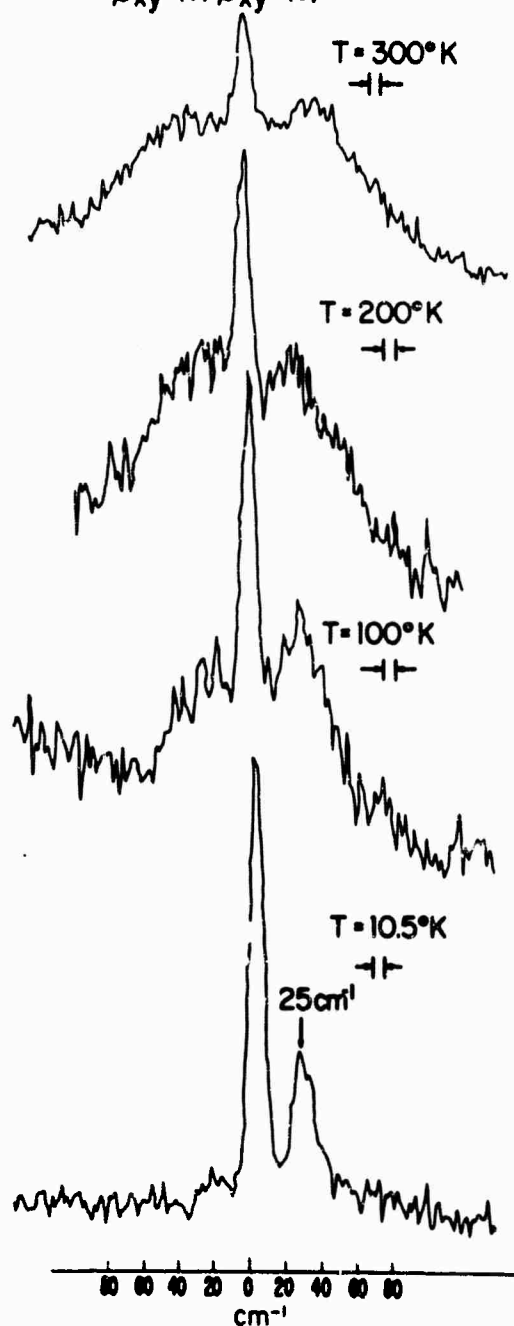cm⁻¹   cm⁻¹

Fig. 5-8 High frequency sideband data for KCl:OH⁻. Stokes
shifts are to the right.

scattering geometries look very much alike with a peak on either side
of the trace position. In addition for both samples, the $\langle \beta^v_{xx}(t)\beta^v_{xx}(0)\rangle$
component has a line on the <u>low</u> energy side of the trace position shifted
by a few wave numbers. As the temperature is lowered, the $\langle \beta^v_{xx}(t)\beta^v_{xx}(0)\rangle$
scattering gradually collapses into the trace position until there is a
single line at the stretching frequency. The $\langle \beta^v_{xy}(t)\beta^v_{xy}(0)\rangle$ component
at low temperatures shows a single line shifted from the stretching mode
by 25 cm^{-1} for KCl:OD$^-$ and 32 cm^{-1} for KCl:OH$^-$. A search was made
for the "300" cm^{-1} lines which have been seen by I.R. experiments and
reported in section IV of this paper. This line was not observed at any
temperature or in any scattering geometry in both samples.

C. Discussion of the Sideband Results

The KCl:CN$^-$ and KBr:CN$^-$ systems can be explained by assuming
the barrier to rotational motion is small so that at room temperature
the CN$^-$ molecule can be expected to induce Raman scattering similar
to that induced by a free rotator. As the temperature is lowered, the
effects of the crystalline potential become more and more significant
until the temperature is finally below the barrier energy, and the scat-
tering becomes more characteristic of some other type of motion than
that of a free rotator. We shall discuss the low temperature spectra
in terms of a Devonshire model for the molecular motion. The free
rotator energies for a linear molecule are given by[38] $H_{rot} = B J(J+1)$
where J is the angular momentum quantum number and B is propor-
tional to the inverse of the moment of inertia (if $B = h/8\pi^2 cI$ and all
quantities are in cgs units H_{rot} is in cm^{-1}). Each level is $(2J+1)$ fold
degenerate. For the linear molecule the selection rules for the vibrating

THE ROTATIONAL RAMAN EFFECT: MOLECULAR

IMPURITIES IN ALKALI HALIDES

By

R. Callender and P. S. Pershan

Technical Report No. ARPA-39

Contract ARPA SD-88

January 1970

Submitted to:

Advanced Research Projects Agency

The Department of Defense

Division of Engineering and Applied Physics

Harvard University

Cambridge, Massachusetts

rotator are $\Delta J = 0, \pm 2$ for the Raman scattering and $\Delta J = \pm 1$ for infrared absorption. Transitions involving $\Delta J = 0$ are called the Q branch, $\Delta J = +2$ the S branch, $\Delta J = -2$ the O branch, $\Delta J = +1$ the R branch, and $\Delta J = -1$ the P branch.

In the Raman effect one sees scattering results from the Q, S and O branches which are both linearly polarized parallel or perpendicular to the incident electric field of the laser beam. The scattering intensities have been worked out for this case by Minck et al.[39] In particular it is shown that the unshifted scattering (i. e. the Q branch) has two components. For scattered light polarized parallel to the laser electric field, we designate this component as $Q_{\parallel}$, and the other scattering polarization we designate as $Q_{\perp}$. Minck explicitly derived for the free rotator case that $Q_{\parallel}$ results largely from the trace component plus a small component due to traceless parts of the molecular frame polarizability tensor. For $Q_{\perp}$ only traceless scattering can be observed. Minck shows that the traceless components in both $Q_{\parallel}$ and $Q_{\perp}$ contribute an order of magnitude or more less intensity than that contributed by the trace component of $Q_{\parallel}$.

The shape of the Raman S and O branches is largely determined by the thermal population of the J levels. The probability of occupation of a given J manifold increases as the degeneracy, $(2J + 1)$, but decreases by the Boltzmann factor. There is thus a maximum occupied J level and a maximum appears in the spectrum for S and O branches. Very often the simple approximation that the intensity of a given transition is determined solely by the occupation of a given rotational level can be used (see, for example, ref. (40), p. 127, and Minck et al[39]).

Assuming this the separation of the maxima in the S and O branches is. in cm^{-1}, $\Delta SO^{max} = 2\sqrt{8BkT/hc} = 4.70\sqrt{BT}$ with B in cm^{-1} and T in degrees Kelvin. Similarly for the infrared P and R branches $\Delta PR^{max} = \sqrt{8BkT/hc}$ which is just a factor of two smaller than ΔSO^{max}.

The results at high temperatures in Figures 5-3 and 5-4 for KBr:CN⁻ and KCl:CN⁻ do give the features described by the free rotator. First, the data presented in the figures is due to scattering light polarized perpendicular to the laser electric polarization (this is evident as there the trace scattering is reduced by approximately two order of magnitudes from what it would be if polarizers were not used). The $\langle \hat{e}^V_{xx}(t)\hat{e}^V_{xx}(0)\rangle$ and $\langle \hat{e}^V_{xy}(t)\hat{e}^V_{xy}(0)\rangle$ spectra represent different crystal geometries. For a free (isotropic) rotator, these two spectra would be identical. Thus, the differences in the shape and form of these functions give a measure of the anisotropy due to the 0_h environment of the molecule. At the higher temperatures, however, the curves are very similar. Second, the Q scattering is small and is estimated to be about two orders of magnitude smaller for these depolarized spectra then the trace scattering. It should be remembered that some of the apparent Q scattering may result from spurious trace scattering. A third feature in support of this model is that the separation between the two peaks in the Raman results are about twice those of the infrared results. Here we have for $2\Delta PR^{max}$ for KCl:CN⁻ and KBr:CN⁻ respectively, at $300^\circ K$, 82 cm^{-1} and 72 cm^{-1}. [2] In the Raman measurements ΔSO^{max} is approximately 61 and 59 respectively at $300^\circ K$.

The peak separation is a relatively sensitive measure of the free rotator model. As given by the equation above, the peak separation is

proportional to the square root of the temperature. In Figures 5-9 and 5-10 the separation has been plotted as a function of the square root of the temperature for KBr:CN⁻ and KCl:CN⁻ respectively and for both scattering geometries. At low temperatures when the scattering from the low energy side of the stretching mode is too small to be seen, the peak separation has been taken as double the value of the high energy peak's shift. Also, the $\langle \hat{e}^V_{xy}(t)\hat{e}^V_{xy}(0)\rangle$ scattering for KCl:CN⁻ ceases to have any definable peak structure near 120°K, and has thus not been plotted for $T \leq 120^\circ$. It is evident at some temperature, ~100°K for KCl:CN⁻ and ~60°K for KBr:CN⁻, there is a significant departure from the predicted straight line. Further, even at room temperature and worse at the lower temperatures, the peak separations for the two scattering functions are not equal. There is an indication that they will become equal at some higher temperature near 400°K. It can be concluded from these figures that even at room temperature the crystalline environment of the molecule significantly modifies the free rotational states and, further, that the interactions are slightly larger in KCl:CN⁻ than KBr:CN⁻.

The parameter B can be measured for the CN⁻ molecule by taking the slopes of the lines in Figures 5-9 and 5-10. A different B for each polarization is found. In the obvious notation, we have for KCl:CN⁻, $B_{xxxx} = .6$ cm⁻¹ and $B_{xyxy} = .9$ cm⁻¹, and KBr:CN⁻, $B_{xxxx} = .4$ cm⁻¹ and $B_{xyxy} = .7$ cm⁻¹. These agree reasonably well with $B = 1.0$ cm⁻¹ for KCl:CN⁻ and $B = .8$ cm⁻¹ for KBr:CN⁻ from the reported infrared data. [2, 41] The errors in measuring the S and O peak separations determine the error in the value of B. An error of

Fig. 5.9 Energy separation between the peaks on the Stokes and anti-Stokes side of the Q(0) position as a function of temperature for KBr:CN$^-$.

PEAK SEPARATION

KCℓ + .53 % CN⁻

$\frac{3}{4} < \beta^{\nu}_{xx}(t)\,\beta^{\nu}_{xx}(0) >$

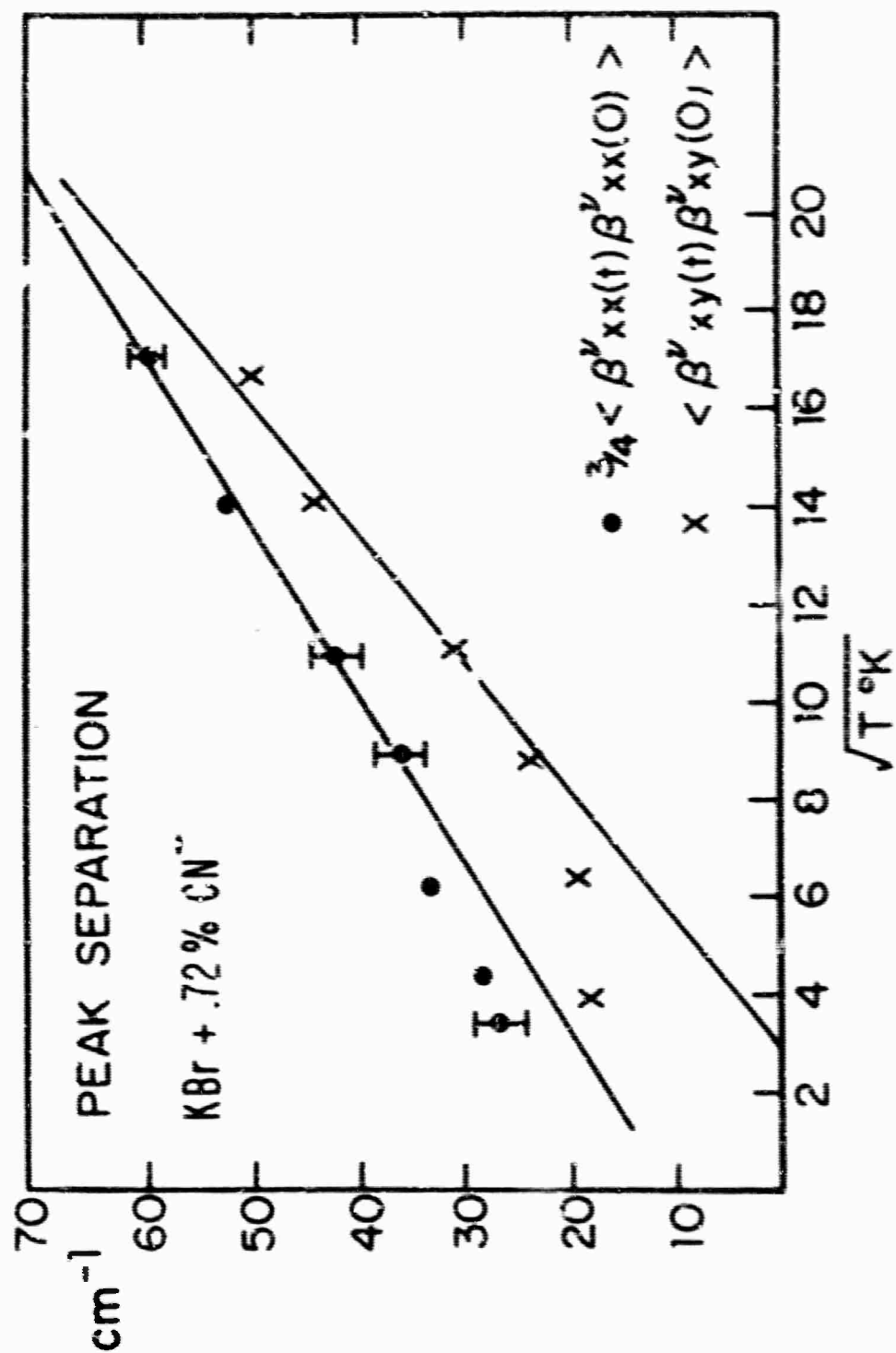$< \beta^{\nu}_{xy}(t)\,\beta^{\nu}_{xy}(0) >$
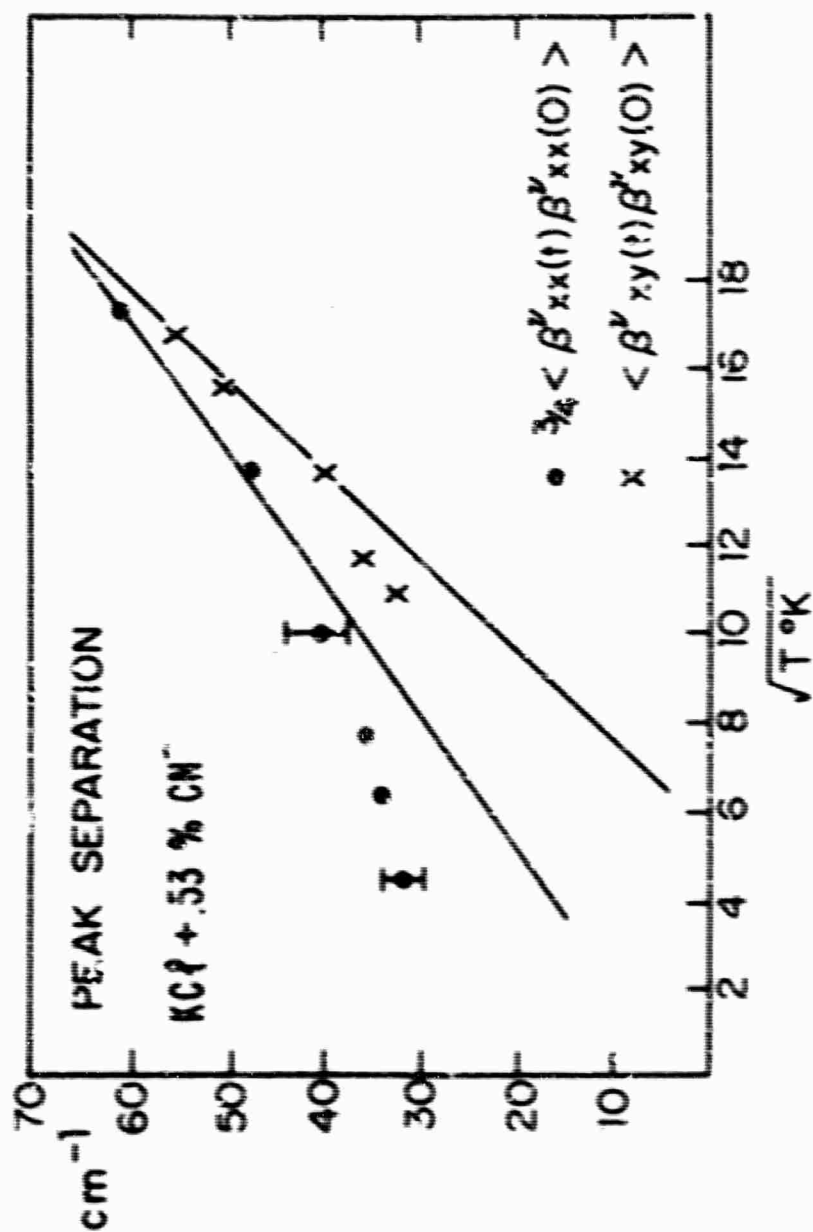
cm⁻¹

$\sqrt{T\,°K}$

Fig. 5-10 Energy separation between the peaks of the Stokes and anti-Stokes side of the Q(0) position as a function of temperature for KCl:CN⁻.

about 20% can be assumed. The value of B is characteristic of the
molecule and all of the above measured numbers should agree. The
discrepancies are due to measureing inaccuracies and, more importantly,
to the effects of the crystal environment on the free rotational states.
It is clear from the data that the crystalline environment has the effect
of decreasing the measured value. We shall use the value of $B = 1.0$ cm^{-1}
in the discussion below.

The rotational fine structure which is just within our resolution
(separation $\approx 4B \approx 4$ cm^{-1}) was not observed here nor in the I.R. results.[2]
Only the envelope functions of the various branches are seen. This may
be due to a broadening of the rotational lines due to the coupling with
the lattice or due to small unresolvable splitting of the higher energy
states of the rotational levels by the crystal field or some combination.

Let us now turn our attention to the low temperature data. Here
it is necessary to take explicit account of the interaction of the molecule
with the lattice. Reasonable success can be obtained using the Devonshire
model.[1,4] It is assumed that the center of mass of the molecule is tied
to a lattice point and the host ions are at rest so that the effect of the
host is to produce a static potential which is totally symmetric under O_h
symmetry. The form of the Devonshire potential is

$$V(\theta,\phi) = -\frac{K}{8}(3 - 30 \cos^2\theta + 35 \cos^4\theta + 5 \sin^4\theta \cos 4\phi) \qquad (5-1)$$

where K is a constant. From a simple perturbation calculation one
finds that each of the $(2J + 1)$ fold degenerate J^{th} rotational states is
split into levels which are labeled according to the irreducible represen-
tation of O_h. Sauer[42] has recently improved the calculation, but for the
small fields here, Devonshire calculations[1,4] are satisfactory.

In Figure 5-11a the results have been plotted as a function of the parameter $K(K \geq 0)$ in units of B. For K = 0 the solutions reduce to the rotator states. For K positive, the potential minima are in the six (100) directions and the maxima are in the eight (111) directions. The difference between potential maxima and potential minima is about 1.7 K.

The selection rules for Raman scattering are that the cross product of the initial and final state must contain either A_{1g}, E_g, or F_{2g} symmetry component (see section IV). It was shown in section II that the A_{1g} component (diagonal and independent of crystal orientation) corresponds to trace scattering, the E_g component (diagonal, but traceless) to $\langle \beta^v_{xx}(t)\beta^v_{xx}(0)\rangle$, and the F_{2g} component (off diagonal) to $\langle \beta^v_{xy}(t)\beta^v_{xy}(0)\rangle$. The cross sections for the various transitions have not been calculated for the Devonshire model; however, it seems reasonable to assume that transitions which satisfy $\Delta J = 0, \pm 2$ would be the strongest in this case of a weak crystal field. Similarly for the infrared absorption experiments, the cross product must contain T_{1u} (i.e. the symmetry of a vector quantity, the dipole operator) with the added hypothesis again of $\Delta J = \pm 1$.

Using the KBr:CN⁻ as a particular example, there is a reasonably well-defined line at 13 cm⁻¹ in the spectrum recorded at 12°K having E_g-like symmetry. Outside of the six very low energy states the first transition having any E_g symmetry is $F_{1u}(J = 1) \rightarrow F_{1u}(J = 3)$. Assuming B = 1.0 cm⁻¹ and assigning this to the 13 cm⁻¹ line we have $K \approx 20$. In Figure 5-11b the important Devonshire levels have been plotted for K = 20. The near infrared absorption measurements indicate
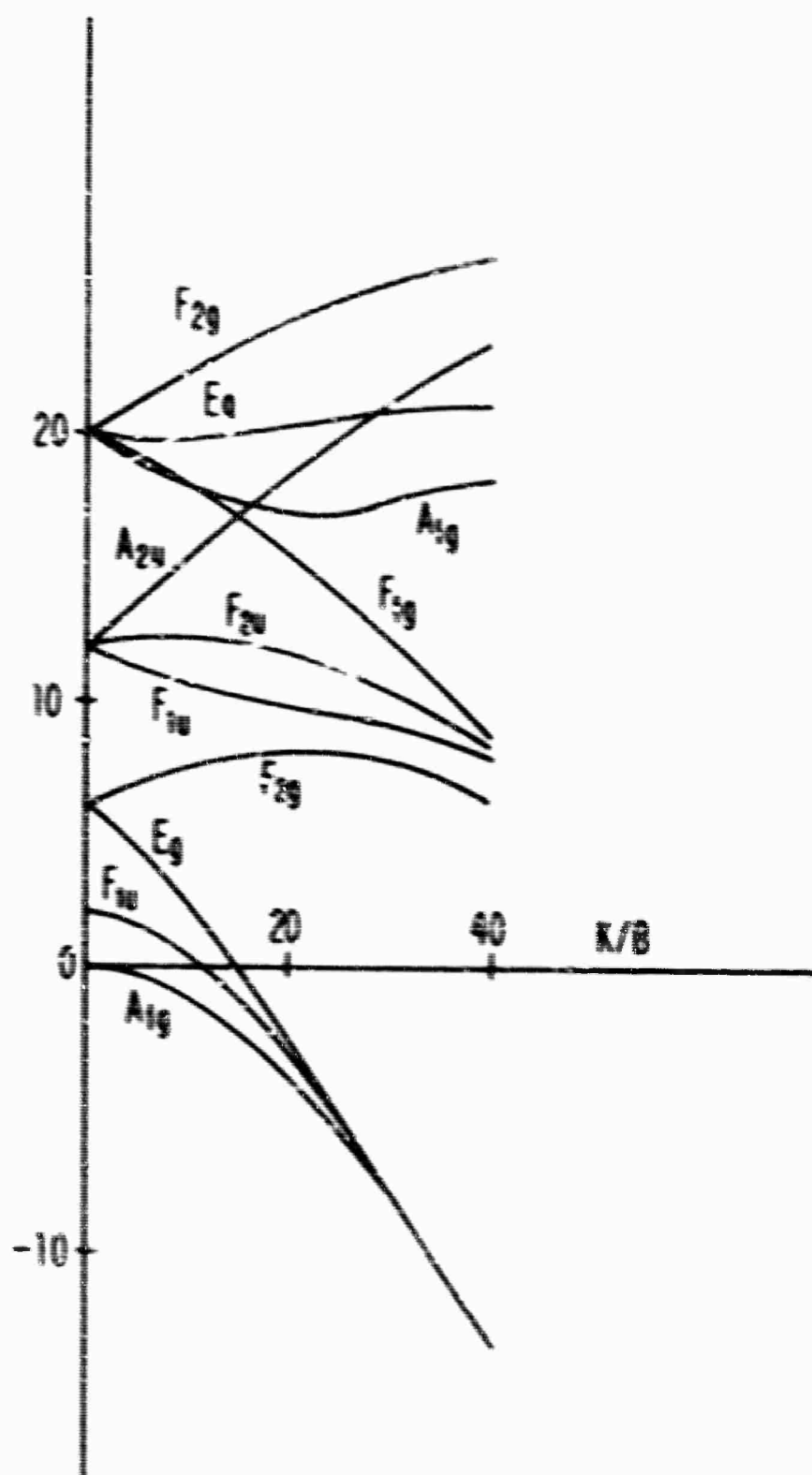
Fig. 5-11a Devonshire energy levels for $K = 6$.

CM^{-1}

17.0 ——— F_{1u} (J = 3)

15.3 ——— F_{2g} (J = 2)

14.7 ——— F_{1u} (J = 3)

12.3 ——— F_{2g} (J = 2)

1.7 ——— E_g (J = 2)

1C ——— F_{1u} (J = 1)

0 ——— A_{1g} (J = 0)

KBr : CN$^-$
K = 20

1.1 ——— E_g (J = 2)

.4 ——— F_{1u} (J = 1)

0 ——— A_g (J = 0)
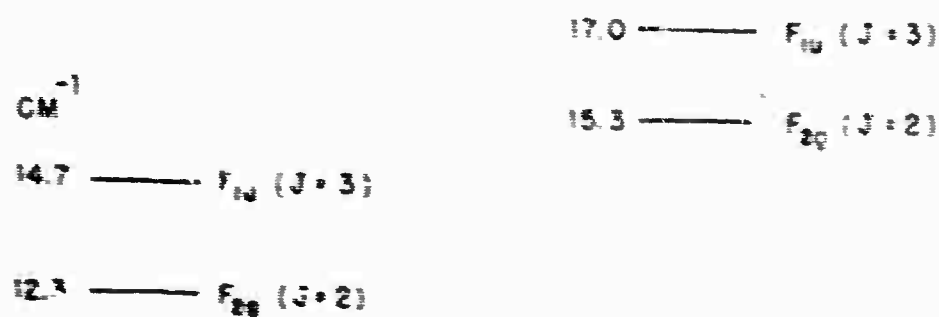
KCl : CN$^-$
K = 27

Fig. 4-18. Devonshire levels for KBr:CN$^-$ and KCl:CN$^-$.

there is a low energy transition at 12 cm^{-1}.[2] Assuming this belongs to the transition of $F_{1u}(J = 1) \rightarrow F_{2g}(J = 2)$, at K = 20, the Devonshire model predicts this transition to be at 11.3 cm^{-1}. The other Raman structure seen in the $(\delta^V_{xy}(t)\delta^V_{xy}(0))$ scattering is not too well defined, but is centered at roughly 11 cm^{-11}. Since this is of F_{2g} symmetry, it can be fitted to $A_{1g}(J = 0) \rightarrow F_{2g}(J = 2)$ having a value of 12.3 cm^{-1}. The width of this line may be due to a phonon interaction or to a small amount of translational motion of the molecule. As the temperature at which the Raman measurements were made was about $10^\circ K$, the transition $A_{1g}(J = 0) \rightarrow E_g(J = 2)$ and the inverse $E_g(J = 2) \rightarrow A_{1g}(J = 0)$ should have been seen for $(\delta^V_{xx}(t)\delta^V_{xx}(0))$ scattering. The width of these transitions for K = 20 is $\approx 3 \, cm^{-1}$ centered about the Q(0) frequency. Measurements taken with a resolution of 2.5 cm^{-1} were taken at $12^\circ K$ to observe these transitions. In the case of KBr:CN⁻ for $(\delta^V_{xx}(t)\delta^V_{xx}(0))$ scattering, a line about 30% broader than the resolution of the instrument was seen, and in KCl:CN⁻¹ a line with the width of the instrument was seen. Probably, as discussed above, there is a residual trace scattering masking these transitions. In the infrared at $2^\circ K$ the linewidth of the Q(0) mode is 2.5 cm^{-1}.[1] In this case the width is due to $A_{1g}(J = 0) \rightleftharpoons F_{3e}(J = 1)$ and about 2.0 cm^{-1} wide at K = 20. Subtracting their[2] resolution of .6 cm^{-1} and the Raman measured width of the stretching mode (from the trace scattering results) of .4 cm^{-1}, we are left with a result in good agreement with the tunneling level spacings predicted on the basis of the Devonshire model.

Similar arguments can be made for KCl:CN⁻. Here, the line observed with the $(\delta^V_{xx}(t)\delta^V_{xx}(0))$ symmetry at 16 cm^{-1} suggests a

slightly larger value for K, i.e. $k \approx 27$. The $K = 27$ Devonshire levels have been plotted in Figure 5-11b.

If we then take the difference in the maxima and minima of the potential to be some measure of the barrier height, then $V_B = 1.7$ $K = 34$ cm^{-1}(52°K) for KBr:CN$^-$ and $V_B = 46$ cm^{-1}(70°K) for KCl:CN$^-$. It can be noted that these characteristic temperatures agree quite well with the temperatures at which the peak separations in Figures 5-9 and 5-10 begin to deviate from a ΔT dependence (about 60°K for KBr:CN$^-$ and 100°K for KCl:CN$^-$).

The NaCl:CN$^-$ results in Figure 5-5 show entirely different scattering phenomenon. The results can be understood in terms of a harmonic torsional oscillation about one of the six equivalent ⟨100⟩ axes of the crystal where occasionally the molecule hops from one ⟨100⟩ direction to another 100 direction. The first motion gives $\langle \bar{\alpha}^v_{xy}(t)\bar{\alpha}^v_{xy}(0)\rangle$ scattering and the hopping process will predict the $\langle \bar{\alpha}^v_{xx}(t)\bar{\alpha}^v_{xx}(0)\rangle$ results.

In the torsional harmonic oscillator model, the molecule oscillates about a fixed center of mass making an instantaneous angle ξ with one of the ⟨100⟩ directions. In the harmonic approximation, the molecule has a potential energy of the form

$$V(\xi) = \frac{1}{2} \frac{(\omega^{lib}_0)^2}{2B} \xi^2 \tag{5-2}$$

where ω^{lib}_0 is the librational (or torsional) frequency in cm^{-1}. To be rigorous, it should be noted that the two angles are necessary to specify the wave functions. If the molecule is in the crystal z direction, we could pick the two angular coordinates to be one angle measured from

the z axis in the xz plane and a second angle measured in the yz plane. In general these two angular coordinates are not independent variables. As a first approximation, however, if the angular deviations are sufficiently small they may be treated as though they are independent. The problem then reduces to considerations of two independent simple harmonic oscillators.

Picking to be the angular deviation of the molecule in the xz plane, then to first order the change in the polarizability tensor has components

$$\delta a_{xz} = (a_{zz} - a_{xx})\bar{z} . \tag{5-3}$$

The diagonal components are changed only to second order. Here a_{xx} and a_{zz} are the components of the polarizability tensor of the molecule aligned along the z axis. In the notation of section II, $(a_{zz} - a_{xx}) = (b - a)$. Thus, the Raman scattering from this type of motion is allowed and is completely off diagonal giving $\langle E^{\vee}_{xy}(t)E^{\vee}_{xy}(0)\rangle$ scattering.

Using the virial theorem, we have

$$\langle \frac{1}{2} \frac{(\nu^{lib}_0)^2}{2B} z^2 \rangle = \frac{1}{2} \nu^{lib}_0 (n + \frac{1}{2}) \tag{5-4}$$

where n is the occupation state of the librator. Thus

$$\langle z^2 \rangle = \frac{2B}{\nu_0} (n + \frac{1}{2}) . \tag{5-5}$$

For the ground state, then $z_{rms} = \sqrt{2B}$. 14 and for the first excited state $z_{rms} = \sqrt{3} \cdot$. 14 when $\nu_0 = 54$ cm^{-1} and $B = 1$ cm^{-1}. These angles are not too large to significantly invalidate the small angle approximation (i.e. $z_{rms} \gg z^2_{rms}$).

Assuming now the molecule is well localized along one of the
(100) directions, the diagonal components will have a time dependence
because at different times the molecule changes from one (100) direc-
tion to another. This could occur in one of two ways: either the mole-
cule is thermally activated and "hops" over some sort of a potential
barrier or there is quantum mechanical tunneling through the barrier.
The latter process can be neglected here because the linewidths of
the $\langle \mathcal{E}^V_{xx}(t)\mathcal{E}^V_{xx}(0)\rangle$ scattering decrease with decreasing temperature.
Generally, tunneling processes depend upon high symmetry for their
existence. At high temperatures, the point site symmetry is reduced
in a random way due to the phonon structure of the crystal. As the
temperature is reduced the reduction of symmetry is lessened and
tunneling probabilities would increase, thus broadening the
$\langle \mathcal{E}^V_{xx}(t)\mathcal{E}^V_{xx}(0)\rangle$ line (i.e. instead of having six degenerate states,
the tunneling transitions would split some of this degeneracy).

If the quantum mechanical approach is supplemented by a semi-
classical argument where $\langle \mathcal{E}^V_{xx}(t)\mathcal{E}^V_{xx}(0)\rangle$ is viewed as a correlation
function, then the effects due to a "hopping" process can be calculated
in the following manner. The correlation function is defined as

$$\langle \mathcal{E}^V_{xx}(t)\mathcal{E}^V_{xx}(0)\rangle = \sum [\mathcal{E}^V_{xx}(t)][\mathcal{E}^V_{xx}(0)]p(\mathcal{E}^V_{xx}(t), \mathcal{E}^V_{xx}(0)) \qquad (5\text{-}6)$$

where the summation is intended to be over all possible values of $\mathcal{E}^V_{xx}(t)$
and $\mathcal{E}^V_{xx}(0)$. Also $[\mathcal{E}^V_{xx}(t)]$ is the value of $\mathcal{E}^V_{xx}$ at time t and p(A, B)
is the joint probability function. Defining the function p(A|B) as the
probability of A given that B has occurred (i.e. the conditional pro-
bability), the p(A, B) = p(A|B)p(B) is a basic consequence of any

Markoffian process. Define the combination of terms St to mean the "S^{th} direction at time t". In this case the molecule can have any one of the $\pm x \langle 100 \rangle$ directions. We shall use the convention that if x is a particular S^{th} direction then -S means the $-x$ direction. Then, $p(St|S_0O)$ means the probability the molecule is in the Sth direction at time t when it is given the molecule was in the S_0^{th} direction a $t = 0$.

If it is assumed that the hopping process in Markoffian so that the probability distribution of molecular orient: t time t is determined by the orientation at time $t - dt$, . $|S_0O)$ can be easily determined. This is a relatively common approximation which has been used to describe a number of physical systems. See, for example, ref. (43). Letting $A_{SS'}$ be the probability per unit time, the molecule hops from the Sth direction to the S' direction. $A_{SS'}$ will be a constant independent of time in this approximation. Also under this assumption, the following equation is then evident for small Δ':

$$p(S, t + \Delta t|S_0O) = \sum_{S' \neq S} p(S't|S_0O)A_{SS'}\Delta t + p(St|S_0O) - \sum_{S' \neq S} p(St|S_0O)A_{SS'}\Delta t. \tag{5-7}$$

Expanding

$$p(St + \Delta t|S_0t_0) = p(St|S_0t_0) + \frac{dp(St|S_0t_0)}{dt}\Delta t + \ldots \tag{5-8}$$

the following is obtained

$$\frac{dp(St|S_0t_0)}{dt} = \sum_{S' \neq S} p(S't|S_0t_0)A_{SS'} - p(St|S_0t_0) \sum_{S' \neq S} A_{SS'}. \tag{5-9}$$

The first term represents the probability of the molecule hopping into the S direction from any of the others, and the second term is for the

probability of hopping out of the S direction. Picking a solution of the form e^{Mt} reduces the above equation to solving a six by six secular determinant. This can be significantly simplified by noting the following. From the symmetry of the lattice, it is clear that there are only two independent hopping probabilities/unit time. For a molecule in a given direction, it can hop to either an orientation that is 90° or 180° from the original. Thus, let $A_{S,S'} \equiv A(S' \neq -S)$ and $A_{S,-S} \equiv C$. Further it is evident there are only three independent conditional probability functions, namely $p(St|S0)$, $p(St|S'0)(S' \neq \pm S)$ and $p(-St|S0)$. This reduces the secular equation to a 3 × 3 which has two parameters. The solutions are

$$p(St|S0) = \frac{1}{6}(1 + 2e^{-6A|t|} + 3e^{-(4A+2C)|t|}) \qquad (5\text{-}10)$$

$$p(-St|S0) = \frac{1}{6}(1 + 2e^{-6A|t|} - 3e^{-(4A+2C)|t|})$$

$$p(St|S'0) = \frac{1}{6}(1 - e^{-6A|t|}) \ . \qquad S' \neq \pm S$$

Note these solutions give the proper boundary conditions, namely $p(S0|S0) = 1$ and $p(S'0|S0) = p(-S0|S0) = 0$.

Assuming all $\langle 100 \rangle$ directions are initially equally probably at $t = 0$, we have $p(S0) = 1/6$ for all S. Then by taking the proper average over all $\langle 100 \rangle$ directions

$$\langle \beta^v{}_{xx}(t)\beta^v{}_{xx}(0) \rangle = \frac{2}{9}(a - b)^2 e^{-6A|t|} \qquad (5\text{-}11)$$

where a and be are the components of the CN^- polarizability tensor in the molecular frame as given in section II. Taking the Fourier transform, we have

$$\frac{1}{2\pi}\int_{-\infty}^{\infty} dt\ e^{-i(\omega+\omega^{V})t}\langle \beta^{V}_{xx}(t)\beta^{V}_{xx}(0)\rangle = \frac{1}{9\pi}(a-b)^2 \frac{12A}{(\omega+\omega^{V})^2 + (6A)^2}. \quad (5\text{-}12)$$

This is a Lorentzian line, whose full width at half intensity is 12A in units of sec^{-1}, centered at the stretching mode frequency. Note that the spectra of the scattered light does not depend on the parameter C: this involves "hops" of 180° and does not change the polarizability tensor. The $\langle\beta^{V}_{xx}(t)\beta^{V}_{xx}(0)\rangle$ scattering, then, is a measure of the hopping probability from one $\langle 100\rangle$ direction to another at right angles.

In this semiclassical approach one considers the moleucle as jumping over a potential barrier whose maximum is V_B. For a particular molecule which may be jumping from say the $\hat{x}$ direction to the $\hat{y}$ direction, Chandrasekhar has derived a formula which can be used to determine A (re . (43), p. 70). Taking v^{lib}_0 to be in cm^{-1} and A in sec^{-1}, if c is the speed of light in $cm\ sec^{-1}$

$$A = (2\pi)^{-1}c\ v^{lib}_0\ \exp[-V_B/kT].$$

This predicts an exponential dependence of the half width of $\langle\beta^{V}_{xx}(t)\beta^{V}_{xx}(0)\rangle$ scattering on inverse temperature. In Figure 5-6 the $\langle\beta^{V}_{xx}(t)\beta^{V}_{xx}(0)\rangle$ half width has been appropriately plotted in units of cm^{-1} and we see that this functional form is well obeyed. In terms of this theory the ordinate should correspond to $12A\ c^{-1}$. From the slope of this curve, $V_B = 395^{\circ}K$ can be determined. Using the measured value for v^{lib}_0, the simple formula above predicts a value for $(2\pi)c^{-1}A$ of 54 cm^{-1} at infinite temperature. Taking a twelfth of the infinite temperature intercept in Figure 5-6 and multiplying by 2π, $2\pi c^{-1}A = 52\ cm^{-1}$. The agreement is quite good.

The KCl:OH and KCl:OD⁻ systems in Figures 5-7 and 5-8 are more difficult to understand than the CN⁻ systems. Since the two polarizations for both samples in the high temperature results are nearly identical and resemble S and O branches, it would seem at first sight that perhaps a free rotator model may apply. This is not the case for three reasons. First, the free rotator in the KCl:OH system would have a peak separation of 230 cm^{-1}. Here we have used a value for B = 18.0 cm^{-1} as has been recently suggested for the first excited vibrational state of OH⁻ by Klein et al.[36] The measured value of about 75 cm^{-1} does not agree even approximately. In the second place, the infrared absorption data in the vicinity of the stretching mode at 300° does not show the characteristic P and R branches of a free rotator; a single broad line centered somewhere near the Q(0) position is observed. Thirdly, the peak separation of a free rotator is proportional to the inverse square root of the moment of inertia. That is $\Delta SO^{max} \sim B^{\frac{1}{2}} \sim I^{-\frac{1}{2}}$. Thus, since $(I_{OD}/I_{OH})^{\frac{1}{2}} = 1.375$ (assuming the internuclear spacing of the molecule does not vary with the hydrogen isotope used), it can be expected that $(\Delta SO^{max})_{OH}/(\Delta SO^{max})_{OD} = 1.375$. The measured value of the two samples at 300°K for the $(\Phi^{y}_{xx}(0)\Phi^{y}_{xx}(0))$ component is 70/73 ~ 1 within experimental error.

The helium temperature measurements, on the other hand, could, to some extent, be understood in terms of a harmonic torsional oscillator as in the case of the NaCl:CN⁻ system. The polarization of the shifted sideband has the correct off diagonal symmetry of a librational mode. If the harmonic potential that the molecule sees is written as

$V(\theta) = \frac{1}{2} D\theta^2$ where, as in the NaCl:CN$^-$ system, θ is the instantaneous angle made with one of the $\langle 100 \rangle$ directions, it can be assumed that to first order D is not affected by the isotope change. An examination of the form of the potential in the discussion of NaCl:CN$^-$ shows in this case that $(\nu^{lib}_0)_{OH}/(\nu^{lib}_0)_{OD} = 1.375$. The measured value of $32/25 = 1.28$ is in good agreement. Here we also have $\theta_{rms} = (\frac{18}{32})^{\frac{1}{2}} = .75$ for the ground libration state of OH$^-$ and a somewhat higher value for the OD$^-$ system. This is quite a large value, and the assumptions of such a simple model are not expected to be particularly accurate.

It would appear that the hydroxyl interaction with the lattice is different in different temperature regions. Molecular motion in high temperature regions seems to be governed mostly by an interaction with the translational motion of the molecule as there is no apparent isotope shift. At low temperatures, however, there is a very definite isotope shift and it would seem that the molecular motion involves mostly rotational effects.

The line down shifted from the Q(0) position by a few wave numbers in both the KCl:OH$^-$ and KCl:OD samples is probably due to a clustering effect. It has the correct scattering symmetry (i.e. $\langle \delta^y_{xx}(t)\delta^y_{xx}(0)\rangle$) to be a cluster of two hydroxyl ions one each on adjacent anion sites pointing towards each other along a $\langle 100 \rangle$ direction.

ACKNOWLEDGMENTS

REFERENCES

1. R. Callender and P. S. Pershan, Phys. Rev. Letter 23, 947 (1969).

2. W. D. Seward and V. Narayanamurti, Phys. Rev. 148, 463 (1966).

3. C. H. Chau, M. V. Klein, and B. Wedding, Phys. Rev. Letters 17, 521 (1966).

4. Brent Wedding and Miles V. Klein, Phys. Rev. 177, 1274 (1969).

5. D. R. Bosomworth, Solid State Comm. 5, 681 (1967).

6. W. E. Bron and R. W. Dreyfus, Phys. Rev. Letters 16, 165 (1966) and Phys. Rev. 163, 304 (1967).

7. G. Feher, I. Shepherd, and H. B. Shore, Phys. Rev. Letters 16, 500 (1966).

8. I. D. Shearer and T. L. Estle, Solid State Comm. 4, 239 (1966).

9. R. S. Scott, "Microwave Spectroscopy of Hydroxide Doped Alkali Halide Crystals," thesis, University of Illinois, Urbana, Illinois (1969).

10. U. Kuhn and F. Lüty, Solid State Comm. 2, 281 (1964).

11. H. Paus and F. Lüty, Phys. Status Sol. 12, 341 (1965).

12. F. Lüty and K. F. Weinmann, Bull. Am. Phys. Soc. 12, 82 (1967).

13. V. Narayanamurti, W. D. Seward, and R. O. Pohl, Phys. Rev. 148, 481 (1966).

14. A. F. Devonshire, Proc. Roy. Soc. (London) A153, 601 (1936).

15. G. Placzek, Z. Physik 70, 84 (1931).

16. M. Born and K. Huang, Dynamical Theory of Crystal Lattices (Oxford, Clarendon Press, (1956).

17. R. Loudon, Adv. in Phys. 13, 423 (1964).

18. N. X. Xinh, "Impurity Induced Lattice Infrared Absorption and First Order Raman Scattering of Light by Dielectric Crystals," Westinghouse Research Laboratories, Paper 65-9F5-442-P8 (Pittsburgh, Pennsylvania, 1965).

19. A. A. Maradudin, Solid State Physics, Vol. 19, ed. F. Seitz and D. Turnbull, Academic Press, Inc., New York, 1966, p. 1.

20. See for example, Charles Kittel, Introduction to Solid State Physics, John Wiley and Sons, Inc., New York, 1956, 2nd edition p. 90.

21. See for example, R. Callender, The Rotational Raman Effect: Molecular Impurities in Alkali Halides, thesis, Harvard University, 1969 (unpublished).

22. G. Benedek and G. F. N. Nardelli, Phys. Rev. 154, 872 (1967).

23. R. T. Harley, J. B. Page, Jr. and C. T. Walker, Phys. Rev. Letters 23, 922 (1969).

24. K. A. Valiev and L. D. Eskin, Opt. i Spektros Koprya 13, 262 (1962) [translation Opt. Spectry. (USSR) 13, 505 (1962)] ibid 12, 758 (1962)].

25. R. G. Gordon, J. Chem. Phys. 43, 1307 (1965).

26. A. R. Edmonds, Angular Momentum in Quantum Mechanics, Princeton University Press, Princeton, New Jersey, 1957.

27. M. E. Rose, Elementary Theory of Angular Momentum, John Wiley and Sons, Inc., New York, 1957.

28. E. P. Wigner, Group Theory and its Application to the Quantum Mechanics of Atomic Spectra, Trans. J. J. Griffin, Academic Press, Inc., New York, 1959.

29. P. K. Chang, Brad Lacina, and P. S. Pershan, Phys. Rev. Letters 17 755 (1966).

30. W. B. Lacina, Phonon Optical Properties of Mixed Fluorite Systems, thesis, Department of Physics, Harvard University, 1966.

31. F. Rosenberger, The University of Utah, private communication.

32. B. Fritz, F. Lüty, and J. Anger, Z. Physik 174, 240 (1963).

33. R. London, Adv. in Phys. 14, 421 (1965).

34. T. Timusk and M. V. Klein, Phys. Rev. 141, 662 (1965).

35. T. Timusk, Department of Physics, McMaster University, Hamilton, Ontario, Canada, private communication.

36. M. V. Klein, B. Wedding, and M. A. Levine, Phys. 180, 902 (1969).

37. W. R. Fenner and M. V. Klein, "Raman Scattering by the Hydroxyl Ion in Alkali Halides," in Light Scattering Spectra of Solids, ed. George B. Wright, Springer-Verlag, New York, 1969.

38. G. Herzberg, _Molecular Spectra and Molecular Structure_,
D. Van Nostrand Company, Inc., Princeton, New Jersey, 1950,
Second Edition, Vol. I.

39. R. W. Minck, E. E. Hagenlocker, and W. G. Rado, "Considera-
tion and Evaluation of Factors Influencing the Stimulated Optical
Scattering in Gases," Research Paper, Ford Motor Co., Physics
Department, 1966.

40. G. Herzberg, _Spectra of Diatomic Molecules_, D. Van Nostrand
Company, Inc., New York, Second Edition, 1950.

41. In Ref. (2), the reported value for $KBrCN^+$ was $B = 1.25$ cm^{-1}
and $b = 1.0$ cm^{-1} for $KCHCN^+$ when they used some of the same
formula for ΔPR^{max} as in the text on their data. However,
using their data, we calculate the values reported here.

42. P. Sauer, J. Chem. Phys, 36 (1964).

43. _Selected Papers on Noise and Stochastic Processes_, ed. N. Wax,
Dover Publications, Inc., New York, 1954.

DOCUMENT CONTROL DATA - R & D

Security classification of title, body of abstract and indexing annotation must be entered when the overall report is classified

1. ORIGINATING ACTIVITY (*Corporate author*) Division of Engineering and Applied Physics Harvard University Cambridge, Massachusetts 02138	2a. REPORT SECURITY CLASSIFICATION Unclassified 2b. GROUP

3. REPORT TITLE

THE ROTATIONAL RAMAN EFFECT: MOLECULAR IMPURITIES IN ALKALI HALIDES

4. DESCRIPTIVE NOTES (*Type of report and inclusive dates*)

Interim technical report

5. AUTHOR(S) (*First name, middle initial, last name*)

R. Callender and P. S. Pershan

6. REPORT DATE January 1970	7a. TOTAL NO. OF PAGES 83	7b. NO. OF REFS 43
8a. CONTRACT OR GRANT NO. ARPA SD-88 b. PROJECT NO.	9a. ORIGINATOR'S REPORT NUMBER(S) Technical Report No. ARPA-39	
c. d.	9b. OTHER REPORT NO(S) (*Any other numbers that may be assigned this report*)	

10. DISTRIBUTION STATEMENT

Reproduction in whole or in part is permitted by the U. S. Government. Distribution of this document is unlimited.

11. SUPPLEMENTARY NOTES	12. SPONSORING MILITARY ACTIVITY

13. ABSTRACT

     Raman scattering of light from representative alkali halide crystals containing CN^-, NO_2^-, OH^- and OD^- impurities is reported and analyzed. The observed spectra have a low frequency range, in which the scattered light is usually shifted from the incident light by less than 300 to 400 cm^{-1}, and a high frequency range in which the shifts are typically 1000 to 2000 cm^{-1}. Although the low frequency region does not readily lend itself to quantitative analysis it is clear that its main features can be interpreted in terms of a mixture of second order scattering from the pure host, impurity induced first order scattering that results from perturbing the pure host, and scattering from the rotational degrees of freedom of the molecular impurity.

     The high frequency region, on the other hand, consists of spectra whose frequencies are characteristic of the internal normal coordinates of the molecule. A very narrow totally polarized line with depolarized sideband structure is generally observed. The sharp central component is at the frequency of an internal molecular normal coordinate and, typically, has a linewidth of one cm^{-1}. It is little affected by the type of host or changes in temperature. It is found that the sideband structure gives a measure of the molecule rotational dynamics. Depending on host and impurity, the observed characteristic behavior varies from nearly free rotation to heavily trapped librational motion.

     The techniques employed here, both theoretical and experimental, demonstrate and define the rather broad usefulness of the Raman effect in studying systems of an analogous nature as in, for instance, molecular motion in liquids and liquid crystals as well as molecules in solids.

KEY WORDS	LINK A		LINK B		LINK C	
	ROLE	WT	ROLE	WT	ROLE	WT
Raman Scattering						
Alkali Halide Crystals						
CN^-, NO_2^-, OH^-, OD^- Impurities						
Molecular Motions						